Université de Montréal

Développement d'un modèle expérimental *in vitro* et analyse d'une cinématique anormale de l'épaule

Par

Patrice Tétreault, MD

Université de Montréal

Faculté de médecine

Mémoire présenté à la faculté des études supérieures

en vue de l'obtention du grade de maîtrise en science biomédicale

Août, 2006

Université de Montréal

Faculté des études supérieures

Ce mémoire intitulé :

Développement d'un modèle expérimental *in vitro* et analyse d'une cinématique anormale de l'épaule

Présenté par :

Patrice Tétreault, MD

a été évalué par un jury composé des personnes suivantes :

M. Newman, Nicholas, MD

président-rapporteur

M. DE GUISE Jacques, PhD.

directeur de recherche

Mme. HAGEMEISTER Nicola, PhD.

Mme. NUÑO Natalia, PhD.

Codirectrices

M. Fernandes, Julio C., MD

membre du jury

Résumé

L'arthropathie de l'épaule secondaire à une déchirure massive de la coiffe des rotateurs (ADC) est une condition incapacitante et prévalente chez les patients âgés. Mieux connue sous les termes « Cuff Tear Arthropathy », l'ACD se manifeste surtout par une incapacité à effectuer des tâches avec élévation du bras. Cette incapacité mimique une paralysie du membre supérieur, d'où provient le terme clinique de "pseudoparalysie". À ce jour, le résultat du traitement de l'ADC par prothèse articulaire demeure imprévisible et sous optimal. Avec pour objectif d'améliorer le traitement de l'ADC, nous avons développé un montage expérimental *in vitro* permettant de simuler la pseudoparalysie sur des épaules de cadavres. Nous avons étudié la cinématique anormale de l'épaule causée par une déchirure massive de coiffe sur huit spécimens cadavériques. Pour ce faire, nous avons d'abords localisé le centre de rotation glénohuméral et ensuite utilisé le système de repérage 3D Fastrack et un système de coordonnées avec axes de références centrés sur le centre de rotation. L'abduction dans le plan de l'omoplate a été reproduite par un mécanisme simulant l'action du deltoïde moyen. L'analyse cinématique a révélé un déplacement latéral et supérieur (vers le haut) significatif du centre de rotation glénohuméral en présence d'une déchirure massive de la coiffe des rotateurs. Nous avons également noté un plus grand besoin en force pour l'élévation du bras pour les 30 premiers degrés d'élévation dans le plan de l'omoplate. Étonnamment, une fois passé la barrière des 30 degrés, le besoin en force est comparable à la force nécessaire pour l'élévation en présence d'une coiffe intacte. Cette première analyse cinématique nous indique que notre modèle *in vitro* simule bien la pseudoparalysie de l'ADC retrouvée en clinique. Les résultats obtenus ont permis de conclure que les structures avoisinantes à l'articulation glénohumérale ont une influence significative sur le besoin en force pour l'élévation du bras. Ceci suggère qu'une modification appropriée de la géométrique de l'humérus proximal permettrait possiblement de diminuer le besoin en force lors de l'initiation de l'abduction et potentiellement aider au traitement de la pseudoparalysie. Les connaissances acquises suite à cette étude permettront peut-être de développer une prothèse mieux adaptée à cette condition.

Mots clés : Coiffe des rotateurs, système de coordonnées, cinématique tridimensionnelle, expérimentation *in vitro*, articulation glénohumérale, centre de rotation glénohuméral.

Abstract

Cuff tear arthropathy (CTA) is a debilitating condition that is more prevalent in the elderly. The typical clinical presentation of CTA is the inability to perform tasks requiring elevation of the arm. This incapacity mimics a paralysis of the extremity, and is therefore also referred to as pseudoparalysis. Unfortunately, the results of treatment of CTA with joint replacement are still variable and sub-optimal. With the ultimate goal of improving the treatment of CTA, we have developed an *in vitro* model to study pseudoparalysis in cadaver shoulders. To analyze shoulder kinematics using this model, we first localized the glenohumeral rotation center (GHRC) on all specimens with a digital reconstruction, and used the Fastrack motion analysis system and a joint coordinate system centered over the GHRC. We then studied the abnormal shoulder kinematics caused by simulated massive rotator cuff tear on eight cadaver specimens. We found a significant lateral and superior displacement of the GHRC, and a greater force requirement to elevate the arm through the first 30 degrees in the scapular plane in the presence of a massive rotator cuff tear. Interestingly, once past the 30 degree barrier, the force required to continue elevating the arm was comparable to the force required with the rotator cuff intact. These results indicate a successful *in vitro* simulation of shoulder pseudoparalysis. Our findings suggest that any alteration of the morphology of the glenohumeral joint that decreases the force requirement for initiation of arm elevation could potentially help in the treatment of a pseudoparalytic shoulder. The knowledge gained through such a study might allow the development of a prosthesis better suited to this condition.

Key words: Rotator cuff tear, shoulder kinematics, cuff tear arthropathy, motion analysis

Table des matières

Liste des tableaux

Liste des figures

Liste des sigles et des abréviations

CRAG	Centre de rotation de l'articulation glénohumérale
GHJCS	Glenohumeral joint coordinate system
GHRC	Glenohumeral rotation center
ISB	International Society of Biomechanics
JCS	Joint Coordinate System
SCAG	Système de coordonnées de l'articulation glénohumérale
3D	Tridimensionnel / Three dimensional

Remerciements

Merci à Annie Levasseur. Grâce à ton sens de l'organisation, ton sérieux et les innombrables heures dédiées à la mise en chantier du projet épaule, tu as établi les bases d'une expertise en cinématique de l'épaule pour le LIO et ses futures gradués.

Merci à Mijanou Jodoin. Mijanou est étudiante en génie. Elle a contribué à l'avancement du projet épaule quant à l'élaboration du montage expérimental lors de son stage au LIO.

Merci à Gérald Parent. Gérald est technicien de laboratoire au LIO. Il a offert son expertise en informatique et un support technique tout au long du projet épaule.

Merci à Arnaud Barré. Arnaud est étudiant à la maîtrise au LIO. Il a contribué au projet épaule en offrant son expertise en programmation informatique et ses connaissances pour l'utilisation du logiciel Matlab.

Merci au Dr Nicholas Newman. Nicholas est le chef du département d'orthopédie au CHUM. Son appui a permis l'achat des spécimens cadavériques par le département et dès lors la mise en chantier de ce projet.

Merci au Dr Natalia Nuño. Natalia est chercheur et professeure à l'ETS-LIO. Natalia est co-directrice de mon projet de maîtrise et a contribué à la réalisation du projet par ses critiques et suggestions tout au long du projet.

Merci au Dr Nicola Hagemeister. Nicola est chercheur et professeure à l'ETS-LIO. Nicola est co-directrice de mon projet de maîtrise. De par son intérêt et son enthousiasme pour ce projet, Nicola a grandement contribué à la conception et la réalisation du projet épaule et permis le développement d'une expertise en cinématique de l'épaule au LIO. De plus, elle supervise d'autres étudiants à la maîtrise dans la poursuite de travaux de recherche reliés au présent mémoire.

Merci au Dr Jacques de Guise. Jacques est chercheur et directeur du LIO. Son appui au projet épaule a permis la mise en commun des connaissances acquises lors de projets antérieurs, l'utilisation des ressources techniques et humaines disponibles au LIO, mais surtout de laisser la chance à un jeune clinicien d'explorer le monde de la recherche et de goûter au plaisir de faire face à l'inconnu.

Chapitre 1: Introduction et revue de la littérature

En 1893, Jules Émile Péan implanta la première prosthèse totale de l'épaule, un implant fait de platine et de caoutchouc, fabriqué par Michael, son ami dentiste (Bankes and Emery 1995)(figure 1.1).

Figure 1.1: Prothèse totale du Dr Péan implantée en 1893.

La prothèse est demeurée en place pendant 2 ans, avant d'être retirée suite à une récidive d'une infection tuberculeuse. Ce n'est qu'au milieu du siècle suivant que le Dr Charles Neer développera un implant qui établira vraiment les bases modernes de l'arthroplastie de l'épaule (Neer 1963). Le premier implant, utilisé pour remplacer la surface articulaire de l'humérus, est monobloque et non-cimenté (figure 1.2).

Figure 1.2 : Prothèse humérale du Dr Neer.

La prothèse est ensuite modifiée en 1974 pour offrir deux grosseurs de tête sur une tige cimentée afin de s'adapter aux variations anatomiques individuelles (Neer 1974). Dr Neer ajoute également une composante glénoïdienne pour la surface articulaire de l'omoplate. Dès lors, le succès de la prothèse de Neer a tracé la voie pour la seconde génération de prothèses d'épaule. Celles-ci offrent une sélection de têtes humérales modulaires fixées à une tige standard. De nos jours, une troisième génération de prosthèses à pour objectif principal de reconstruire parfaitement l'anatomie de l'épaule du patient (Boileau and Walch 1997), et de rétablir une biomécanique normale (figure 1.3).

Figure 1.3 : Prothèse modulaire de troisième génération (Depuy)

Cependant, il existe une pathologie complexe de l'épaule pour laquelle le succès de l'arthroplastie demeure encore à ce jour sous optimal (Neer 1974; Neer, Craig et al. 1983; Arntz, Jackins et al. 1993; Williams and Rockwood 1996; Field, Dines et al. 1997; Zeman, Arcand et al. 1998; Zuckerman, Scott et al. 2000; Baumgarten, Lashgari et al. 2004). Mieux connue sous les termes « Cuff Tear Arthropathy », l'arthropathie de l'épaule secondaire à une déchirure massive de la coiffe des rotateurs (ACD) a été formellement décrite par Neer en 1983(Neer, Craig et al. 1983). Cette condition se manifeste par une perte progressive de fonction de l'épaule, un gonflement intermittent de l'articulation, une douleur modérée, mais surtout par un manque de force et d'endurance (figure 1.4).

Figure 1.4 : Gonflement de l'épaule droite chez une patiente avec ADC.

L'incapacité à effectuer des tâches avec élévation du bras est le principal symptôme. Lorsque très sévère, cette incapacité mimique une paralysie du membre supérieur, d'où provient le terme clinique de "pseudoparalysie" (figure1.5). La pseudoparalysie est le résultat d'un disfonctionnement biomécanique chronique suite à une déchirure massive de la coiffe des rotateurs causant ultimement la destruction de la tête humérale.

Figure 1.5 : Patient avec pseudoparalysie de l'épaule droite.

La coiffe des rotateurs est donc essentielle au bon fonctionnement de l'épaule puisqu'elle assure la stabilité dynamique de l'articulation (Saha 1971; Culham and Peat 1993; Loehr, Helmig et al. 1994; Thompson, Debski et al. 1996; Matsen 2002). Les muscles de la coiffe des rotateurs sont le sous-scapulaire, le sus-épineux, le sous -épineux, et le petit-rond (Figure 1.6) (Matsen 2002).

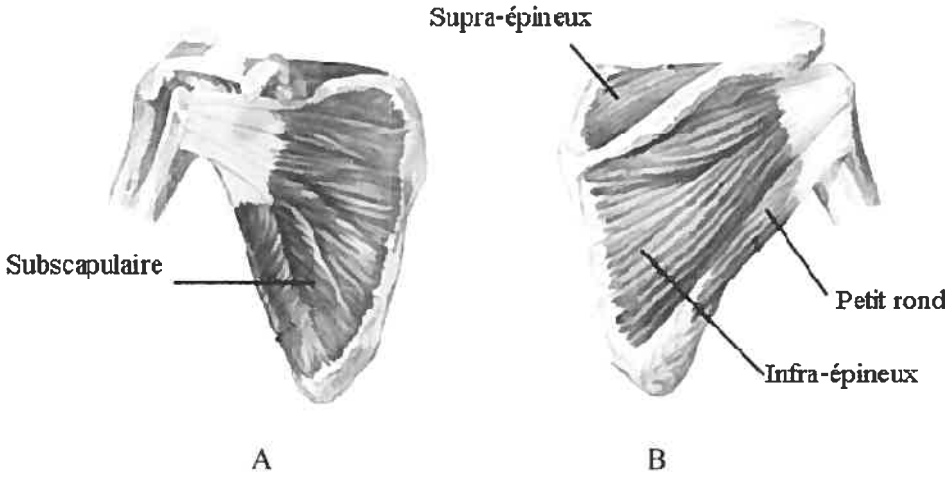

Figure 1.6: Schéma des muscles de la coiffe des rotateurs d'une épaule droite. A- Vue antérieure. B- Vue postérieure.

Les muscles de la coiffe agissent de concert lors des mouvements de rotation et d'abduction du bras en comprimant la tête humérale contre la surface de la glénoïde de l'omoplate (Figure 1.7) (Matsen 2002). Poppen a également analysé les forces résultantes de l'articulation glénohumérale, et démontre que le vecteur résultant est orienté vers le haut lors des 60 premiers degrés d'élévation du bras (Poppen and Walker 1976).

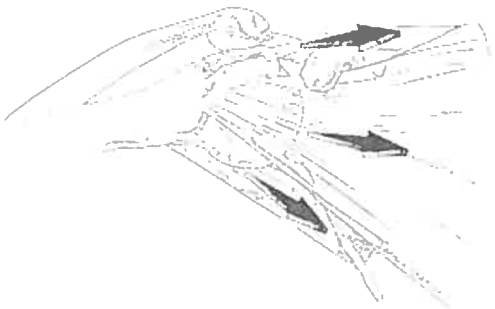

Figure 1.7 : Schéma d'une vue antérieure de l'épaule droite. Action concertée (flèches pleines noires) des muscles de la coiffe des rotateurs lors de l'élévation du bras.

Le muscle deltoïde recouvre les tendons de la coiffe des rotateurs et constitue la principale source de force pour l'élévation du bras (Matsen 2002) (figure 1.8).

Lors de l'abduction du bras dans le plan de l'omoplate, le sus-épineux et le deltoïde s'alignent pour générer une puissance musculaire maximale.

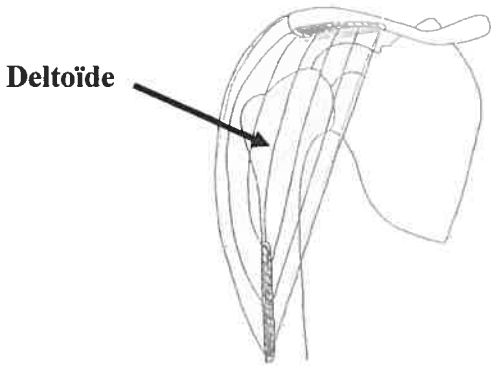

Figure 1.8 : Schéma d'une vue antérieure de l'épaule droite représentant le muscle deltoïde.

Les structures osseuses de l'épaule sont l'omoplate, l'humérus et la clavicule (Figure 1.9)(Matsen 2002). L'omoplate et la clavicule se joignent ensemble par le biais de l'articulation acromioclaviculaire, et permettent de rattacher le membre supérieur au thorax par le biais des articulations scapulothoracique et sternoclaviculaire. L'humérus s'articule avec l'omoplate pour former l'articulation glénohumérale. Ces quatre articulations donnent toute la flexibilité et l'amplitude de mouvement nécessaire au bon fonctionnement dynamique de l'épaule (Matsen 2002).

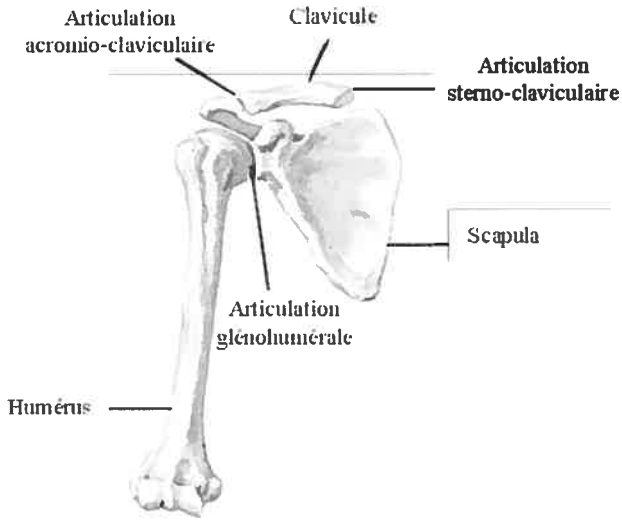

Figure 1.9: Structures osseuses et articulations de l'épaule.

Toutefois, la morphologie osseuse de l'omoplate est telle qu'elle contraint le tendon du sus-épineux à glisser sous l'acromion et l'arche coracoacromial lors de son excursion (figure 1.10). Lorsque le bras s'élève au maximum, l'insertion du tendon du sus-épineux se retrouve pincé entre la surface humérale et l'arche coracoacromial. Cet accrochage répétitif constitue un des facteurs mettant ce tendon à risque de déchirure.

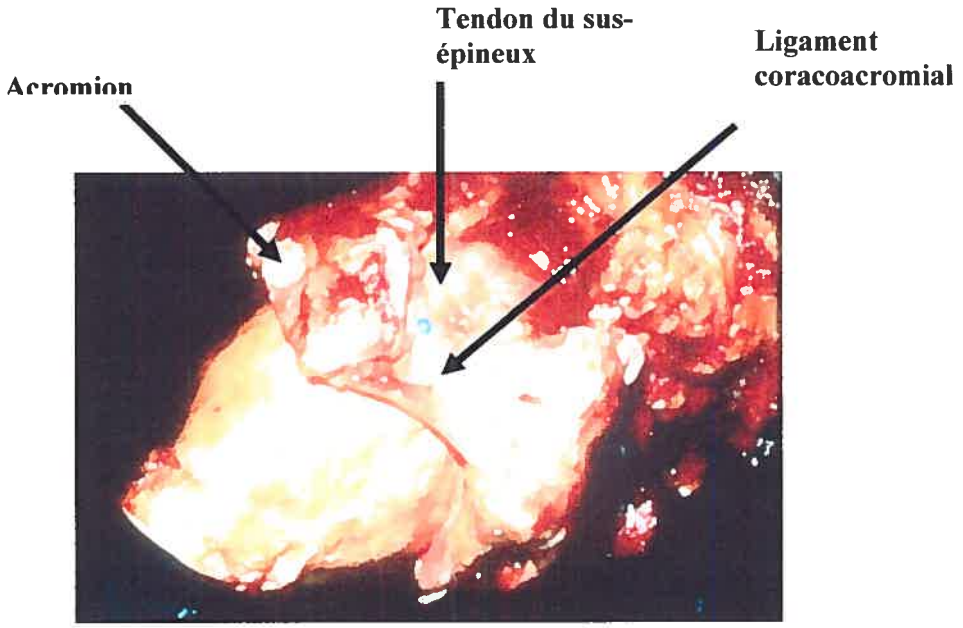

Figure 1.10 : Photo de l'insertion (point bleu) du tendon du sus-épineux passant sous l'arche coracoacromial.

Lorsque la coiffe des rotateurs est déchirée de façon chronique, les tendons se rétractent et la portion musculaire s'atrophie et s'infiltre de graisse. Il devient alors impossible de rattacher les tendons à l'humérus. De plus l'infiltration graisseuse est irréversible et les muscles demeurent avec une perte de puissance significative (Goutallier, Postel et al. 1994; Goutallier, Postel et al. 2003) (Figure 1.11).

A

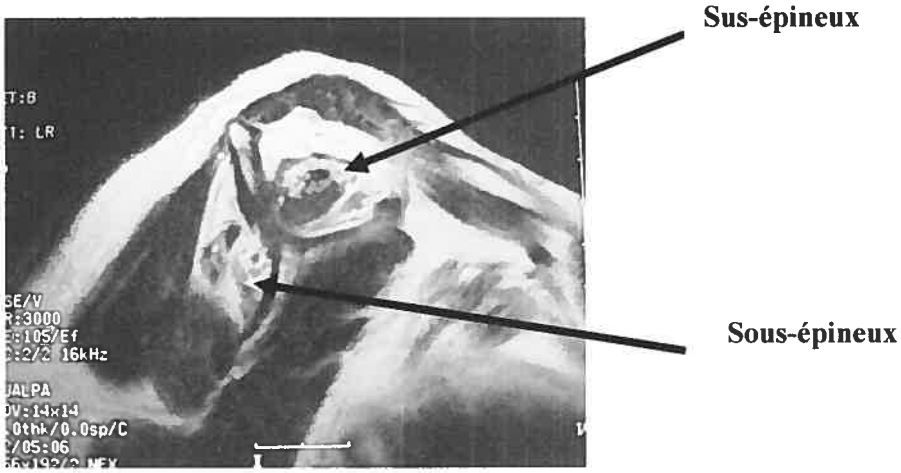

B

Figure 1.11 : Résonance magnétique de l'épaule droite. A- Vue antéropostérieur. Atrophie et rétraction du muscle sus-épineux (flèche vide). Contact entre la tête humérale et l'acromion (tête de flèche vide). Migration proximale du centre de rotation (flèche pointant vers le haut). B- Vue latérale. Atrophie sévère du sus-épineux et du sous-épineux.

Selon Neer (1983), l'instabilité suite à une déchirure massive de la coiffe des rotateurs permet un mouvement de translation glénohumérale anormal, et une migration proximale progressive de la tête humérale (Neer, Craig et al. 1983). Cette migration résulte de l'action du deltoïde et d'une coiffe incompétente. La tête humérale se bute ultimement à l'acromion de l'omoplate. Ce contact incongru entre

la tête humérale et l'acromion accélère l'usure du cartilage, altère la fonction, et accentue la douleur.

Selon des études plus récentes, la dégénérescence du cartilage de l'humérus et de la glénoïde sont en lien direct avec la présence d'une déchirure de coiffe, quoique l'étendue de la déchirure n'a pas de lien directe avec l'étendue des dommages cartilagineux (Hsu, Luo et al. 2003). Feeney (2003) a étudié 33 épaules cadavériques et observé la coiffe et les surfaces articulaires pour des changements dégénératifs. L'atteinte du cartilage était deux fois plus fréquente dans le groupe avec déchirure de coiffe (Feeney, O'Dowd et al. 2003). À cette explication mécanique, Neer (1983) joint une explication nutritionnelle du fait qu'une déchirure de coiffe permet l'extravasation du liquide synovial (Neer, Craig et al. 1983). Cette fuite diminue la quantité et la qualité de l'apport nutritionnel de ce liquide, ce qui accélère l'atrophie du cartilage et de l'os sous-jacent.

Le diagnostic de l'ADC peut être confirmé par radiographie simple (Hamada, Fukuda et al. 1990) (figure 1.12).

A

B

Figure 1.12 : Arthropathie glénohumérale secondaire à une déchirure massive de la coiffe des rotateurs. A- Vue antéropostérieur d'une radiographie de l'épaule droite. B- Vue axiale d'une radiographie de l'épaule droite.

La migration supérieure de la tête humérale contre la surface de l'acromion est visible ainsi que le pincement de l'articulation glénohumérale. La tête humérale est habituellement déformée avec l'arrondissement de la grosse tubérosité et l'affaissement de la portion articulaire supérieure dans les cas plus avancés. L'érosion des structures avoisinantes telles l'acromion, la clavicule, et jusqu'à la base de la coracoïde peut être très importante. Le rayon x à lui seul peut confirmer le diagnostic, mais l'IRM peut mieux détailler l'étendue de l'atteinte dégénérative de la coiffe. Nove (1996) rapporte que l'étendue de la déchirure de coiffe et la dégénérescence du sous-épineux visible sur IRM, ont un lien direct avec la migration supérieure de la tête humérale (Nove-Josserand, Levigne et al. 1996).

Étant donné que la présentation clinique de l'ACD varie selon la chronicité de cette condition, plusieurs traitements ajustés à la symptomatologie sont disponibles. Ceux-ci incluent, le traitement médical, un lavage arthroscopique (Caporali, Rossi et al. 1994) avec ou sans débridement, la tubéroplastie humérale (Fenlin, Chase et al. 2002; Scheibel, Lichtenberg et al. 2004), l'arthrodèse (Cofield and Briggs 1979; Arntz, Matsen et al. 1991), et l'arthroplastie (Coughlin, Morris et al. 1979; Post, Haskell et al. 1980; Neer, Watson et al. 1982; Neer, Craig et al. 1983; Post 1985; Field, Dines et al. 1997).

Ces dernières années et encore de nos jours, le traitement standard de l'ADC pratiqué par la majorité de chirurgiens demeure l'arthroplastie. Le soulagement de douleur et une restauration minimale de la fonction du bras permettent de reprendre

les activités de base de la vie quotidienne (Neer, Craig et al. 1983; Arntz, Jackins et al. 1993; Williams and Rockwood 1996; Field, Dines et al. 1997; Zeman, Arcand et al. 1998; Zuckerman, Scott et al. 2000; Baumgarten, Lashgari et al. 2004). L'hémiarthroplastie, soit le remplacement de la surface humérale seulement, est préconisée par le fait que la migration proximale d'une prothèse humérale contribue au descellement précoce de la composante glénoïdienne. Ce phénomène est connu sous le nom de "rocking horse glenoid" (Franklin, Barrett et al. 1988; Baumgarten, Lashgari et al. 2004).

Dans les années 70, quelques chirurgiens ont tenté d'adapter le principe de fulcrum fixe de la prothèse de hanche à l'articulation de l'épaule. C'est-à-dire de contraindre l'articulation glénohumérale à une mécanique du type "ball and socket". La force de traction du deltoïde est dès lors convertie en force rotative afin de permettre l'élévation du bras. Malheureusement, ce type de prothèse était voué à l'échec de par son design qui impose une force de cisaillement excessive causant le descellement de la composante glénoïdienne de son interface osseuse. Ces prothèses sont demeurées à titre expérimental et n'ont pas connu d'exploitation commerciale (Coughlin, Morris et al. 1979; Post, Haskell et al. 1980; Post 1985) (Lettin, Copeland et al. 1982).

Neer (1982) avait noté la mauvaise qualité de l'os de l'omoplate chez les patients avec ADC. Selon lui, la mauvaise qualité osseuse ne peut permettre une fixation adéquate de la composante glénoïdienne. Il a lui-même tenté des modifications à la composante glénoïdienne afin de contrer la migration supérieure de la tête humérale. Des composantes élargies, soient 200 à 600 % plus grande qu'une composante standard, n'ont pas apporté de succès significatif (Neer, Watson et al. 1982).

Une étude récente de Orr (1988) à partir d'éléments finis sur des glénoïdes originales et prosthétiques, est en accord avec les principes de Neer (1982) quant au fait qu'un design contraignant a une plus grande prévalence de lignes radiolucente à l'interface os-ciment et un risque de descellement augmenté (Orr, Carter et al. 1988).

Des chirurgiens ont cherché à améliorer les résultats de l'hémiarthroplastie grâce à une composante humérale avec une plus grande surface articulaire afin d'améliorer la congruence entre la tête humérale et l'acromion (prothèse de type CTA- Cuff Tear Arthropathy). De 2000 à 2001, Rockwood a traité 60 épaules avec ADC avec une prothèse de type CTA (DePuy, Warsaw, Indiana) (figure 1.13). En

comparaison avec l'état pré-opératoire, les résultats cliniques ont démontré une amélioration clinique au point de vue de la douleur (4x moins de douleur), amélioration clinique de la rotation externe (3x plus de rotation externe), et amélioration de l'élévation antérieure (2x plus d'élévation) (Visotsky, Basamania et al. 2004). Toutefois, ce type de prothèse ne peut traiter une pseudoparalysie déjà présente cliniquement en pré-opératoire.

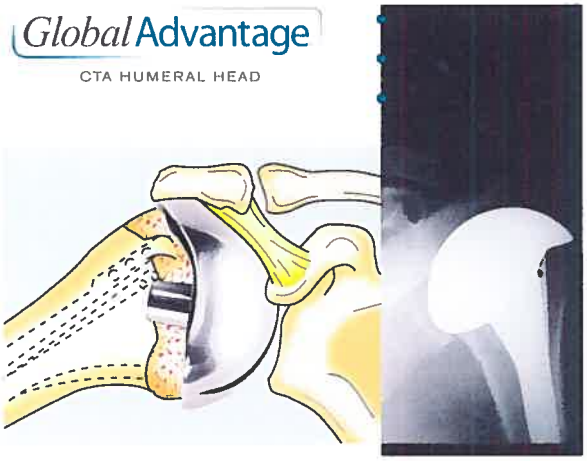

Figure 1.13 : Prothèse "CTA humeral head" de Depuy.

Au début des années 90, le professeur Grammont a réussi à mettre de l'avant une prothèse semicontraignante de type inversée (Grammont and Baulot 1993) (figure 1.14). L'humérus est alors converti en cupule afin de recevoir une glénoïde convertie en sphère. Ce design médialise le centre de rotation glénohuméral et augmente le bras de levier du deltoïde. L'imbrication des composantes rétabli le fulcrum au niveau glénohuméral et permet au deltoïde d'être plus efficace lors de l'élévation du bras.

Figure 1.14 : Prothèse inversé Delta III de Depuy.

La prothèse inversée permet d'éliminer la pseudoparalysie, mais ne peut toutefois redonner une force plus grande en rotation externe et interne. Différents chirurgiens ont publié des résultats cliniques sur des patients opérés avec prothèse inversée. Les indications et les limitations pour l'utilisation de cette prothèse se précisent de plus en plus (Sirveaux, Favard et al. 2004; Boileau, Watkinson et al. 2005; Frankle, Siegal et al. 2005; Werner, Steinmann et al. 2005). La durée de vie de la prothèse n'est pas encore bien définie, mais des signes indirects de descellement apparaissent très tôt autour de la composante humérale, ainsi que des signes d'érosion du rebord inférieur de l'omoplate sous la composante glénoïdienne dès l'année suivant l'implantation (Boileau, Watkinson et al. 2005) (McFarland, Sanguanjit et al. 2006) (Woodruff, Cohen et al. 2003; Nyffeler, Werner et al. 2004).

Depuis ce regain d'intérêt pour les prothèses semicontraingnantes, chirurgiens et scientifiques sont à la recherche d'une fixation plus durable pour la composante glénoïdienne (Ahir, Walker et al. 2004; Nyffeler, Werner et al. 2005), (Murphy and Prendergast 2005), (Harman, Frankle et al. 2005). Nyffeler (2004) note lors d'un examen post-mortem huit mois après l'implantation d'une prothèse inversée Delta III, une encave prononcée au pole inférieur du col de l'omoplate(Nyffeler, Werner et al. 2004). Cette érosion va au-delà de la vis d'encrage inférieure de la composante glénoïdienne. Cette perte osseuse correspond à l'usure de la cupule de polyéthylène.

L'histologie révèle une réaction à corps étrangers dans la capsule, mais aucun signe de descellement. Il poursuit son analyse dans une étude sur huit spécimens cadavériques en testant quatre positionnements différents de la composante glénoïdienne. Il conclut que la composante glénoïdienne fixée avec son rebord inférieur plus bas que le rebord de la surface osseuse de la glénoïde améliore significativement l'adduction et l'abduction(Nyffeler, Werner et al. 2005).

D'autres chirurgiens essaient de mieux comprendre l'impact réel du design d'une prothèse sur la restauration de la fonction. De Wilde (2004) a analysé plusieurs types de prothèses disponibles sur le marché grâce à des simulations sur ordinateur. Il conclut que la prothèse inversée présente le meilleur design donnant au deltoïde le meilleur bras de levier possible (De Wilde, Audenaert et al. 2004). Néanmoins, les cliniciens suggèrent d'utiliser de cet implant avec modération, et recommande même l'implantation que chez les patients de 70 ans et plus, étant donné qu'un style de vie plus sédentaire diminue les risques de descellement.

Étonnamment, certains patients avec déchirure massive de la coiffe des rotateurs ne présentent qu'une douleur légère à modérée, et une amplitude de mouvement quasi complète (figure 1.15).

A

B

Figure 1.15: A- Patient jouant régulièrement au golf malgré des déchirures massives de coiffe bilatérales. B- Patient peu sportif avec déchirure massive de coiffe à l'épaule droite.

En effet, l'évolution clinique à long terme d'une déchirure massive de coiffe demeure imprévisible. Selon Neer (1983), environ 4% des patients avec une déchirure de coiffe évolueront vers l'ADC étant donné que la plupart des déchirures sont petites (Neer, Craig et al. 1983). Hamada (1990) a suivi 22 patients avec déchirure massive de la coiffe traités de façon conservatrice. 5 des 7 patients suivis sur une période de 8 ans ont développé des changements dégénératifs progressifs sur les radiographies (Hamada, Fukuda et al. 1990). Dans une étude rétrospective de 25 patients avec déchirure de coiffe traités par acromioplastie et débridement par arthroscopie et suivi de 6 à 9 ans, 7 patients ont montré des signes cliniques et radiologiques d'ADC (McMahon, Debski et al. 1995).

Selon Apoil (1989), l'ADC s' est développée chez 25% des 56 patients 10 ans après débridement ouvert d'une DMC (Apoil 1989). Rockwood (1995) quant à lui rapporte qu'aucune épaule avec déchirure massive de coiffe sur 53 n'a montré une détérioration de l'articulation glénohumérale après acromioplastie ouverte et débridement de coiffe. Les épaules avec suivi de moins de 5 ans ont été comparées avec les épaules avec un suivi de plus 5 ans. La détérioration fonctionnelle et radiologique n'a pu être associée au facteur temps. Chez tous les patients, les tendons du sous-scapulaire et du petit-rond étaient intacts. Tous les patients ont suivi un programme intense de renforcement de la coiffe, du deltoïde, et des muscles périscapulaires. Même si le sus-épineux et le sous-épineux étaient absents, l'effet compressif de sous-scapulaire, du petit-rond, et l'effet stabilisateur des muscles

périscapulaires ont permis le fonctionnement actif de l'épaule (Rockwood, Williams et al. 1995).

Plusieurs auteurs s'interrogent donc sur l'effet d'une déchirure de coiffe sur la biomécanique de l'épaule (Howell and Kraft 1991; Loehr, Helmig et al. 1994; Bigliani, Kelkar et al. 1996). Encore de nos jours, aucun facteur pronostic n'a été identifié permettant de savoir avec certitude quelle épaule avec une déchirure de coiffe évoluera vers l'ADC.

Inman (1996) a utilisé le concept de couplage des forces "Force Coupling" pour déterminer les forces nécessaires au fonctionnement de l'épaule (Inman, Saunders et al. 1996). Il établit que les forces musculaires dans le plan coronal proviennent du deltoïde avec une force directrice verticale supérieure et une force verticale inférieure par les muscles de la coiffe. La rotation et l'abduction sont possibles grâce à deux forces opposées agissant de chaque côté du centre de rotation. La présence et l'importance de cette force concertée des muscles antérieurs et postérieurs de la coiffe a été démontrée par électromyographie (Saha 1971).

Burkhart (1992) a présenté des patrons de cinématique de l'épaule sous fluoroscopie (Burkhart 1992). Son analyse a permis l'identification de 3 groupes avec fulcrum différent. Un fulcrum instable cause l'altération progressive du couplage des forces transverse et coronale. Le degré d'instabilité correspond directement à l'étendue de la déchirure de coiffe sur le plan antéro-postérieur. Il décrit ensuite un modèle basé sur l'analogie du pont suspendu (Burkhart 1992; Burkhart, Esch et al. 1993; Burkhart, Nottage et al. 1994) (figure 1.16). La localisation des attaches du pont suspendu sur les tubérosités résulte en une cinématique glénohumérale stable ou instable, selon la présence d'une force de couplage transverse intacte.

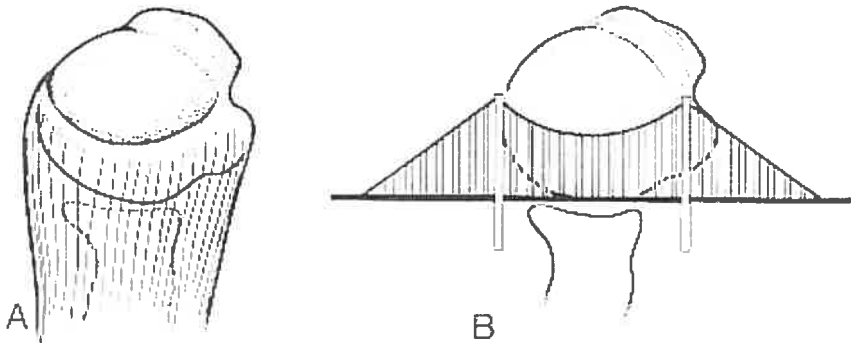

Figure 1.16 : Analogie du pont suspendu présenté par Burkhart (1991). A- Schéma d'une vue supérieure axiale d'une épaule avec déchirure de la coiffe. B- Schéma d'une vue supérieure axiale d'une épaule avec superposition d'un pont suspendu.

D'autres études ont utilisé différents types de montages *in vitro* pour analyser la mécanique de la coiffe des rotateurs(Ovesen and Nielsen 1986; An, Browne et al. 1991; Loehr, Helmig et al. 1994; Debski, McMahon et al. 1995; Halder, Zhao et al. 2001; Kelkar, Wang et al. 2001; Parsons, Apreleva et al. 2002).

Loehr (1994) a utilisé un montage statique pour reproduire l'élévation du bras dans le plan de l'omoplate (figure 2.17). Le mouvement est simulé en déplaçant manuellement un levier inséré dans l'humérus. Ce type de montage soulève toutefois des interrogations en ce qui a trait à la reproduction de la ligne d'action de certains muscles de l'épaule, et à l'utilisation d'un humérus amputé à mi-longueur, ce qui néglige l'impact des propriétés inertielles d'un membre supérieur complet. Il parvient toutefois a démontré qu'une lésion d'aux moins deux tendons (sus-épineux et sous-épineux) est nécessaire pour déstabiliser l'articulation glénuhumérale (Loehr, Helmig et al. 1994).

Ovesen (1986) utilise le même type de montage, soit avec fixation de l'omoplate au niveau de la pointe inférieure (figure 2.17). Cette fixation fait abstraction du mouvement scapulothoracique et de l'inclinaison naturelle de l'omoplate retrouvés *in* vivo. En 1991, An et al. utilisent un système de traction par câbles et détermine à l'aide système de positionnement magnétique l'élévation maximale au niveau glénohumérale s'effectue dans le plan antérieur au plan de l'omoplate (An, Browne et al. 1991) (figure 2.17). Pour obtenir cette élévation maximale, l'humérus doit faire une rotation externe.

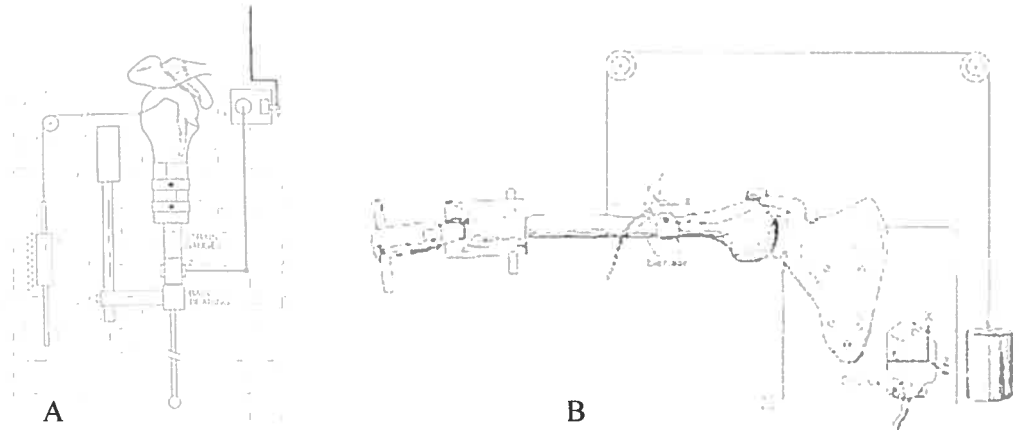

Figure 1.17 : Montages expérimentaux statiques. A- Ovesen (1986), Loehr (1994). B- An (1991).

Afin de reproduire plus fidèlement une cinématique normale de l'épaule, certains auteurs décrivent l'utilisation de montages dynamiques, permettant ainsi de simuler un mouvement d'élévation de façon automatisée (Debski, McMahon et al. 1995; McMahon, Debski et al. 1995; Thompson, Debski et al. 1996; Halder, Zhao et al. 2001; Kelkar, Wang et al. 2001; Parsons, Apreleva et al. 2002) (Figure 1.18). Ces différents montages tentent ainsi de reproduire les lignes d'action des différents muscles.

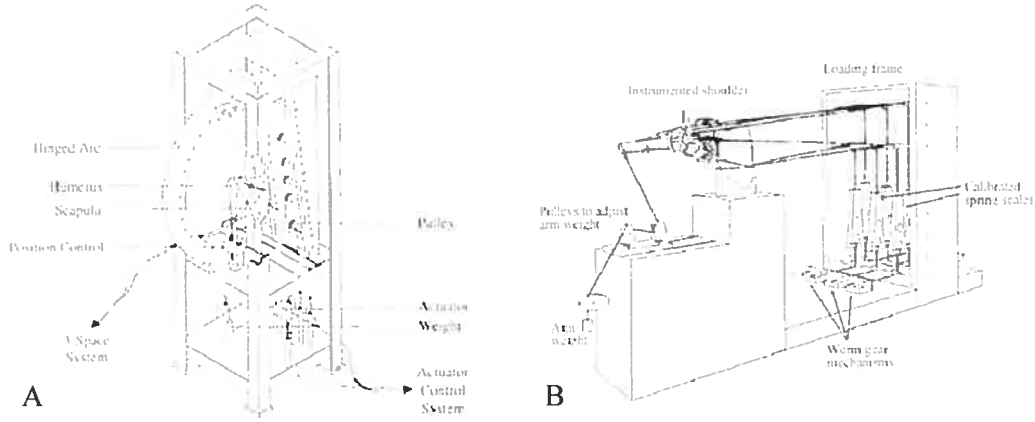

Figure 1.18 : Montages expérimentaux dynamiques. A- Halder (2001). B- Keklar (2001).

Thompson (1996) utilise le même montage que Debski (1995) (figure 2.19). Ce type de montage utilise un membre supérieur entier ce qui permet de simuler plus

exactement les propriétés inertielles retrouvées *in vivo*. De plus, l'inclinaison de l'omoplate est reproduite afin de préserver un positionnement naturel au niveau glénohuméral.

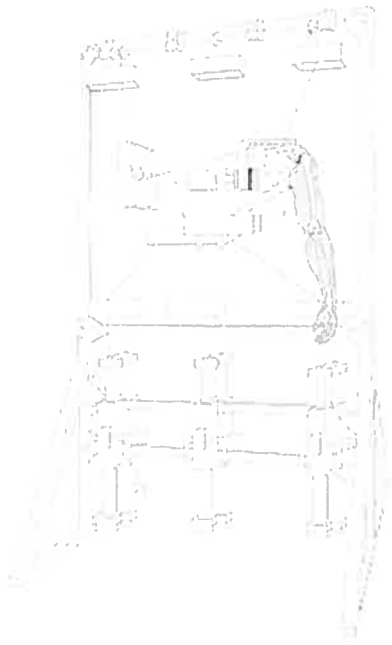

Figure 1.19: Montage expérimental dynamique développé par Debski (1995).

Thompson (1996) démontre alors que des forces de couplages intactes permettent de générer une force compressive suffisante pour maintenir réduite la tête humérale et ainsi préserver une cinématique de type "ball and socket" (Thompson, Debski et al. 1996).

À ce jour, aucune étude n'a spécifiquement analysé, *in vitro*, la cinématique anormale de la pseudoparalysie. Nous sommes convaincus qu'un montage expérimental, permettant ce type d'analyse, permettrait d'identifier précisément sur quels paramètres morphologiques de l'articulation le chirurgien doit intervenir pour prévenir ou traiter la pseudoparalysie de l'ADC.

Il est vrai que les prothèses d'épaule actuelles parviennent à redonner un minimum acceptable de fonction. Toutefois, le rétablissement post-opératoire demeure imprévisible, et inévitablement lié au design et à la survie de l'implant. Dès lors, nous croyons qu'une meilleure connaissance de la cinématique de la pseudoparalysie peut éventuellement mener à la conception d'une prothèse d'épaule mieux adaptée à cette condition et favoriser un rétablissement fonctionnel maximal.

Chapitre 2: Problématique

2.1 Problématique

Premièrement, l'arthropathie glénuhumérale secondaire à une déchirure massive de coiffe des rotateurs (ADC) est une condition incapacitante et son traitement demeure à ce jour sous optimal. Les prothèses d'épaule présentement disponibles parviennent à soulager la douleur mais la récupération fonctionnelle est imprévisible et souvent liée à la longévité de l'implant. Il existe un besoin pour des implants mieux adaptés à cette condition.

Deuxièmement, les connaissances sur la cinématique de l'épaule en présence d'une déchirure massive de la coiffe des rotateurs sont insuffisantes. Il est donc essentiel de développer un modèle *in vitro* capable de simuler la pseudoparalysie de l'ADC afin d'acquérir des données de façon fiable et reproductible.

2.2 Hypothèses de travail

Lors de l'élaboration de ce travail, plusieurs hypothèses ont été sont soulevées concernant l'impact d'une déchirure de coiffe des rotateurs sur la cinématique de l'épaule. La première hypothèse est que la déchirure massive de coiffe des rotateurs change le déplacement du centre de rotation glénohuméral. La seconde est que la force et la cinématique sont affectées.

2.3 But de l'étude

Le but premier de ce travail est donc de développer un montage expérimentale *in vitro* permettant d'analyser la cinématique de l'articulation glénohumérale. Le but second est de simuler une déchirure massive de la coiffe des rotateurs et d'analyser les conséquences sur la cinématique glénohumérale à différents degrés d'élévation du bras.

Chapitre 3: Méthodologie et situation des articles

3.1 Méthodologie

Le premier et le deuxième article de ce mémoire ont déjà été présentés dans la thèse de maîtrise de notre collaboratrice Annie Levasseur. Ces articles décrivent la méthodologie quant à la mise en place du montage, la mise au point de la technique pour définir le centre de rotation glénohuméral, et le processus de familiarisation avec le système de coordonnées et ses axes de référence qui permettront une analyse cinématique.

Le troisième article décrit l'utilisation de notre montage expérimental pour étudier la cinématique anormale de l'épaule causée par la présence d'une déchirure massive de la coiffe des rotateurs.

Annie Levasseur (50%) et moi-même (50%) considérons avoir contribué également à l'avancement et à la réalisation des travaux présentés dans les articles de ce mémoire.

3.2 Résultats

Dans ce mémoire sont présentés, en exclusivité, les résultats de l'analyse cinématique du troisième article.

Chapitre 4: Article I: Comparison between a geometric and a functional method for the estimation of the glenohumeral rotation center

A. Levasseur, P. Tétreault, J.A. de Guise, N. Nuño, N. Hagemeister

Article soumis à la revue «Journal of Orthopedic Research»

4.1 Abstract

According to the literature, the glenohumeral rotation center (GHRC) can be estimated using a geometric or a functional method. The purpose of this research was to evaluate if localization and excursion of the GHRC were affected by the method used. An experiment was carried out on 8 cadaveric shoulder specimens. The localization of the GHRC and its relative three-dimensional (3D) excursion was analyzed using 3D imagery reconstruction and an electromagnetic tracking device. The results revealed a difference in the localization of the geometric and the functional GHRC. Simulated abduction motion in the plan of the scapula demonstrated a statistically significant difference for the GHRC excursion in the transverse plan (Z axis). Understanding the localization and behaviour of each GHRC will be valuable for future work such as the study of cuff tear arthropathy and eventual prosthetic design.

4.2 Introduction

The International Society of Biomechanics (ISB) recently proposed a definition of a joint coordinate system to standardize shoulder joint motion (Wu, van der Helm et al. 2005). This coordinate system was developed using bony landmarks on the scapula and humerus and the glenohumeral rotation center (GHRC). Being a reference landmark for shoulder joint motion analysis, the GHRC needs to be localized precisely. Its position relative to the scapula is very important for the stability of the joint, which is assumed to act as a ball-and-socket (Helm, Veeger et al. 1992; de Leest, Rozing et al. 1996). Changes in the position of the GHRC could ultimately affect estimation of the lever arms of the muscles and therefore modify the interpretation of shoulder kinematics.

Three different methods have been described to estimate the GHRC: geometric method, regression equation method, helicoidal axis method, pivoting algorithm. The geometric method estimates the GHRC as a sphere fitted through the glenoid surface with a radius based on the size of the humeral head (Helm, Veeger et al. 1992). With the regression equation method, the GHRC is estimated as the center of the best-fitted sphere on the glenoid and humeral head (Meskers, van der Helm et al. 1998). The helicoidal axis method and the pivoting algorithm estimate the GHRC

as the optimal pivot point of the humerus relative to the scapula during a movement of the arm (Woltring 1990; Siston and Delp 2006).

The methods used to estimate the GHRC can be classified in two general categories: geometric (based on the bone geometry) or functional (based on the bone movement) (de Leest, Rozing et al. 1996). To the best of our knowledge, there is no in vitro study that compares the different methods in terms of localization and excursion of the GHRC during movement of the arm. Therefore, the aim of our study was to determine the GHRC on cadaver shoulder specimens, using a geometric and a functional method, and to compare their relative localization, their excursion during the abduction motion of the arm and their localization with respect to the center of the glenoid.

4.3 Material and Method

4.3.1 Specimen preparation

Eight fresh-frozen cadaver shoulder specimens including entire arm were used (4 lefts and 4 rights, age range 59 to 87 years). The specimens were stored in a freezer at -20°C and thawed at room temperature for approximately 8 hours before the dissection. All soft tissues were removed except the rotator cuff muscles, deltoid, capsule and ligament structures. The cadaver specimens did not show any musculoskeletal pathology. Two aluminium triangles were fastened with plastic screws on the scapula and the humerus for calibration purposes. After dissection, the specimens were refrozen and then sent for CT scan. From the CT images, a 3D reconstruction of the shoulder was performed with the help of a commercialized software (SliceOmatic,Tomovision, Canada).

4.3.2 Testing device

A testing device made of an abduction guide and two mounting blocks was used to test each shoulder specimen (Figure 4.1). It was entirely made of wood to avoid interference with the tracking device (Fastrak, Polhemus, USA) used to measure shoulder movement. The abduction guide was shaped like a quarter of arch and controlled elevation of the arm in the scapular plane. The main mounting block

was used to fix the scapula with the arm hanging freely between the edges of the abduction guide. The other block was linked to the main block and used to fix a pulling mechanism, which consisted of an electric cylinder (NV-D Series). This mechanism simulated a continuous motion at constant speed with minimal friction. A force transducer (RL 20000 S beam) was fixed at the tip of the pulling mechanism to a fabric strip that simulated the middle deltoid function during arm elevation.

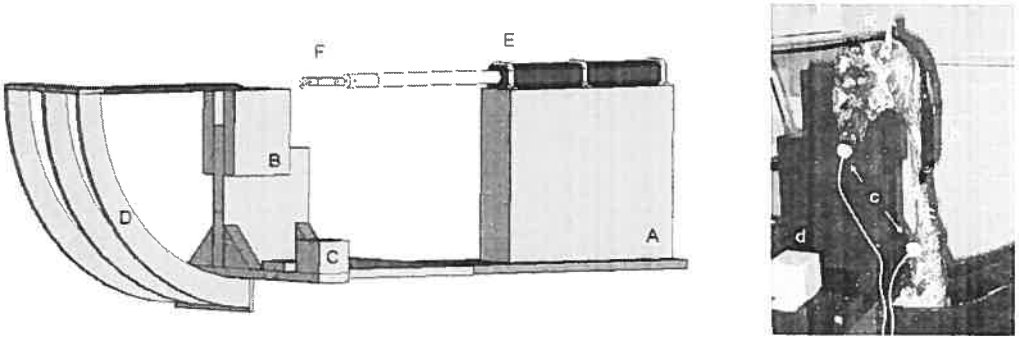

Figure 4.1 : Testing device composed of 2 mounting blocks (A,B); a support for the tracking device (C); a guide (D); and an electric cylinder (E) equipped with a force transducer (F) and positioning of the scapula: (a) scapula guiding device, (b) fabric strip, (c) sensors and (d) transmitter of the electromagnetic tracking device.

4.3.3 Experimentation

Prior to the experiment, each specimen was thawed at room temperature for a period of 12 hours. To immobilize the motion of the forearm, the elbow was fixed with a brass screw. The scapula was mounted on the testing device and positioned such that the medial border of the scapula was perpendicular to the ground. The middle deltoid was resected and replaced by a strip of non-elastic fabric (Figure 4.1). One extremity of the fabric strip was fixed to the deltoid tuberosity, and the other to the pulling mechanism. To prevent slipping of the fabric strip off the acromion, a guiding device was attached on top of the scapula (Figure 4.1). This device also helped in reproducing the line of action of the middle deltoid muscle.

The shoulder joint motion was recorded using an electromagnetic tracking device (Fastrak, Polhemus, USA) (Figure 4.1). The accuracy of the system is 1mm

for linear displacement and 0,1° for angular displacement. Sensors were screwed on plastic plates, which were directly fixed on the scapula and humerus. The sensor on the scapula served as a control for possible movement of the testing device. A personal computer with custom-design software recorded the three dimensional displacement of the arm at 60 Hz in real time.

Before data acquisition, the effect of the environment on the accuracy of the tracking device was evaluated. Then, a calibration procedure was performed which consisted in digitalizing the extremity of both triangles fastened on the scapula and the humerus using a Fastrak pointer. This procedure allowed establishing a transformation matrix between the motion of the cadaver specimen and the virtual 3D reconstruction. Thereafter, 25 passive abduction movements were carried out with the pulling mechanism to condition the specimen and to minimize the viscoelastic effect of the soft tissues(Debski, McMahon et al. 1995; Thompson, Debski et al. 1996; Parsons, Apreleva et al. 2002).

Circumduction movements of the arm were performed by the experimenter over a 30-second period. The experimenter tried not to press the humeral head into the glenoid and not to move the arm beyond the active normal range of motion. Afterwards, 10 abduction movements of maximal range of motion were completed using the pulling mechanism. Each trial lasted 10 seconds. During experimentation, the specimens were kept moist with saline solution. Afterwards, the specimen was restored in the freezer at -20°C.

4.3.4 Method used for determining the geometric GHRC

First, the geometric GHRC was estimated using the 3D computed geometric model of the humerus. A point cloud was selected on this model using the software called Polyworks (InnovMetric, Canada) (Figure 4.2). It corresponds to the articular surface of the humeral head and has the shape of half a sphere (Figure 4.2). The selection was made manually three times by one person. A sphere was then fitted by a least square method to the data of the point cloud (Figure 4.2). The center of this sphere corresponded to the geometric GHRC.

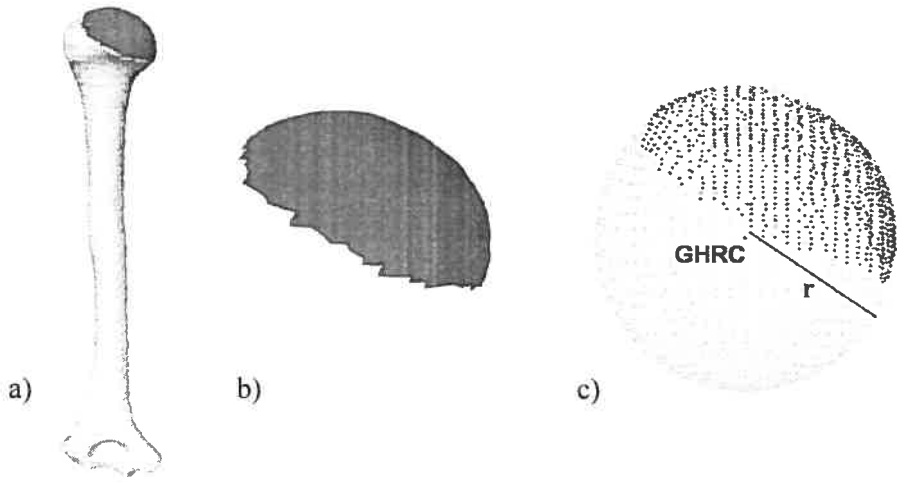

Figure 4.2: (a) Selection of point cloud on the 3D reconstruction of the humeral head; (b) point cloud; (c) sphere estimated by a least square method

4.3.5 Method used for determining the functional GHRC

To estimate the functional GHRC, the method presented by Sinston and Delp was used(Siston and Delp 2006). By a least square method, the GHRC was estimated as a fixed pivot point relative to the scapula during a circumduction movement.

4.3.6 Method used for determining the glenoid center

The glenoid center was determined using the 3D computed model of the scapula. The superior, inferior, medial and lateral edges of the glenoid were labelled with a custom-design computer graphics software (Figure 4.3). The center of the line joining the superior and inferior edges of the glenoid fossa defined the glenoid center in the frontal plane, while the medial and lateral edges defined the glenoid center in the sagittal plane.

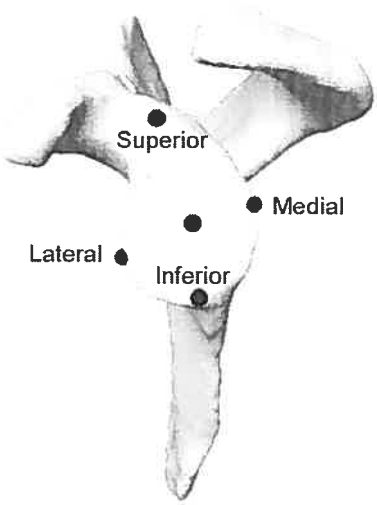

Figure 4.3: Glenoid center determined with the superior, inferior, medial, and lateral edge of the glenoid fossa

4.3.7 Shoulder joint coordinate systems to localize and compare the displacement of the geometric and functional GHRC

The shoulder joint coordinate system used two local coordinate systems: one on the scapula and the other on the humerus. Both local coordinate systems were set by using bony landmarks, as defined by the ISB (Table 4.1) (Wu, van der Helm et al. 2005).

Table 4.1: Bony landmarks for the definition of local coordinate systems

Bone	Anatomical Landmark	Description
Humerus	GHRC	GlenoHumeral rotation center
	EL	Most caudal point on Lateral Epicondyle
	EM	Most caudal point on Medial Epicondyle
Scapula	AC	Most dorsal point on the Acromioclavicular joint
	TS	Triogonum Spinae Scapulae, midpoint of triangular surface on medial border of the scapula in line with the scapular spine
	AI	Angulus Interior, most caudal point of the scapula
	AA	Angulus Acromialis, most latero-dorsal point of the scapula

The reference coordinate system is positioned at the angulus acromialus (AA) of the scapula ($_s$) (Figure 4.4). The Z_s axis is defined as the line connecting TS and AA, pointing to AA. The X_s axis is defined as the line perpendicular to the plane formed by AI, AA and TS. It is pointing forward. The Y_s axis is the common line perpendicular to X_s and Z_s and pointing upward.

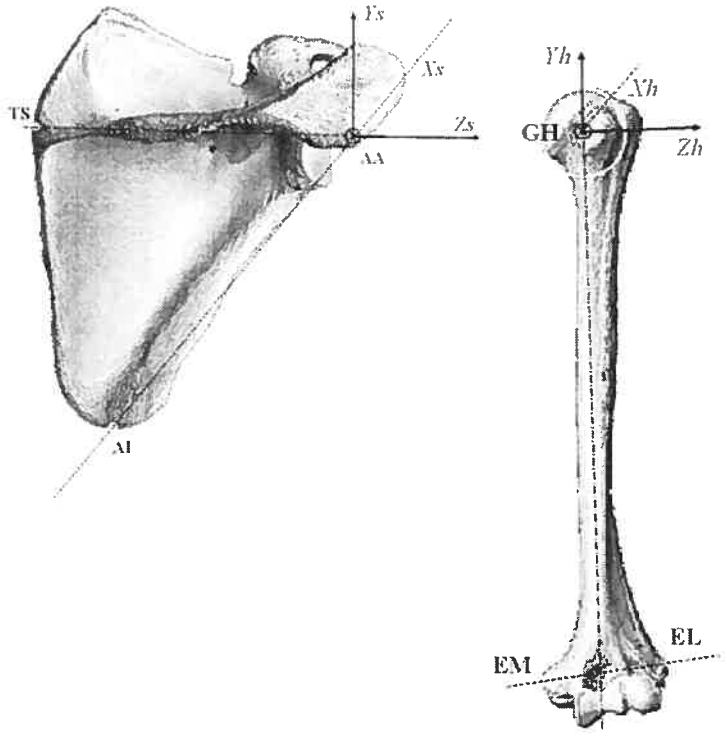

Figure 4.4: Reference and moving coordinate system

The moving coordinate system is positioned at the GHRC of the humerus ($_h$) (Figure 4.4). The Y_h axis is defined as the line connecting GHRC and the midpoint of EL and EM pointing to GHRC. The X_h axis is defined as the line perpendicular to the plane formed by EL, EM and GHRC. It is directed forward. The Z_h axis is the common line perpendicular to Y_h and X_h pointing to EL. The motion of the humerus is described with respect to the scapula coordinate systems using Euler angles (X_h, Z_h, Y_h). Displacement of the geometric and functional GHRC was calculated relative to the AA point on the scapula along 3 axes (X_s, Y_s, Z_s).

4.3.8 Statistical analysis

A two-way ANOVA for repeated measures was performed to determine if there was a difference in displacement between the geometric and functional GHRC during an abduction movement. Statistical significance was set at $\rho < 0,05$. All analyses were performed using the SPSS software.

4.4 Results

The three-dimensional coordinates of the geometric and functional GHRC for each shoulder specimen are presented in table 4.2. The coordinates of the glenoid centers for each specimen in the sagittal frontal and transverse planes are also displayed. All these data represent the actual distance in mm of the GHRC and the glenoid center from the AA point on the scapula along the X_s, Y_s, Z_s.

Table 4.2: Coordinates of the: geometric GHRC, functional GHRC and glenoid center with respect to AA point on the scapula.

	Geometric GHRC			***Functional GHRC***			***Glenoid Center***		
Specimens	*X (mm)*	*Y (mm)*	*Z (mm)*	*X (mm)*	*Y (mm)*	*Z (mm)*	*X (mm)*	*Y (mm)*	*Z (mm)*
1	45.7	-26.7	13.7	40.6	-33.8	12,5	39.1	-19.0	0.0
	± 0.2	± 0.8	± 0.4	± 0.2	± 0.8	± 0.3			
2	37.2	-32.0	4.4	36.4	-35.1	1.2	32.7	-20.8	0.0
	± 0,2	± 0.5	± 0.2	± 0.1	± 0,5	± 0.2			
3	47.0	-17.3	10.3	45.9	-22.3	7.9	41.6	-12.4	0.0
	± 0.1	± 0.1	± 0.1	± 0.1	± 0.1	± 0.1			
4	31.0	-27.7	5.2	29.9	-29.9	8,2	28.1	-20.7	0.0
	± 0.4	± 0.2	± 0.1	± 0.4	± 0.2	± 0.1			
5	46.7	-23.6	3.4	49.8	-22.4	1.4	36.9	-19.3	0.0
	± 0,2	± 0.1	± 0.2	± 0.2	± 0.1	± 0.2			
6	48.5	-24.5	-3.3	50.6	-29.0	-6.6	37.2	-21.5	0.0
	± 0.7	± 0.4	± 0.2	± 0.7	± 0.4	± 0.2			
7	47.1	-36.7	11.7	36.8	-48.6	10.2	36.3	-22.1	0.0
	± 0.1	± 0.1	± 0.0	± 0,1	± 0.1	± 0.0			
8	38.4	-16.3	-1.7	45.0	-20.9	-6.0	27.1	-16.8	0.0
	± 0,0	± 0.2	± 0.1	± 0.0	± 0.2	± 0.1			
Mean	42.7	-25.6	5.4	41.9	-30.3	3.6	34.9	-19.1	0.0
	± 6,3	± 6,9	± 6.1	± 7,2	± 9.1	± 7,3	± 5,2	± 3,2	± 0.0

Referring to Table 4.2, both GHRC were positioned below and in front of the reference landmark AA (Figure 4.5). For the majority of specimens, the GHRC was positioned on the lateral side of AA except for specimen 6 and 8, where both GHRC were positioned on the medial side of AA landmark. Relative to the geometric rotation center, the functional rotation center was lower (4,7 mm) and medially (1,8 mm) positioned.

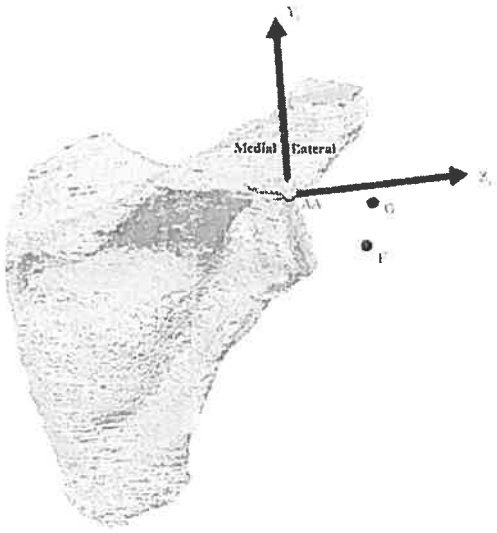

Figure 4.5: Localization of the geometric (G) and functional (F) GHRC for specimen #7.

The excursion of the geometric and functional GHRC during abduction of the arm was calculated. The excursion was defined as the difference between the final and the initial position of the GHRC. Figure 4.6 presents the mean excursion of the geometric and functional GHRC during an average abduction movement of 32,9 ± 7,0°.

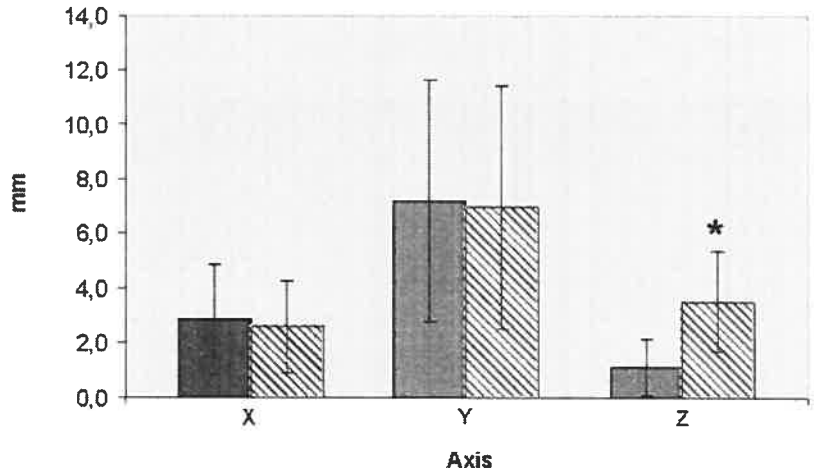

Figure 4.6: Mean displacement of the geometric (plain stick) and functional (lined stick) GHRC.

For the geometric GHRC, its excursion varied between 0,3 to 6,2 mm, 2,0 to 16,3 mm and 0,3 to 3,7 mm in the X, Y and Z axis, respectively. For the functional GHRC, its excursion varied between 0,1 to 5,7 mm, 1,43 to 15,5 mm and 0,4 to 5,9 mm in the X, Y and Z axis, respectively. Based on the statistical analysis, excursion of the geometric and functional GHRC did not differ significantly in the X and Y axis. However, there was a statistically significant difference for the excursion in the Z-axis ($p=0,027$). The functional GHRC moved further lateral relative to the AA point and the geometric GHRC moved further medial to the AA point (Figure 4.7).

At resting position, the distance between both GHRC averaged 3,8 ± 3,4 mm (range 0,8 to 10,3 mm), 5,0 ± 3,3 mm (range 1,2 to 11,9 mm) and 2,6 ± 1,0 mm (range 1,2 to 3,3 mm) in the X, Y and Z axis respectively. In maximum abduction, this distance averaged 3,6 ± 3,2 mm (range 0,2 to 8,6 mm), 4,8 ± 4,0 mm (range 0,4 to 12,7 mm) and 2,4 ± 1,6 mm (range 0,4 to 5,1 mm) in the X, Y and Z axis respectively.

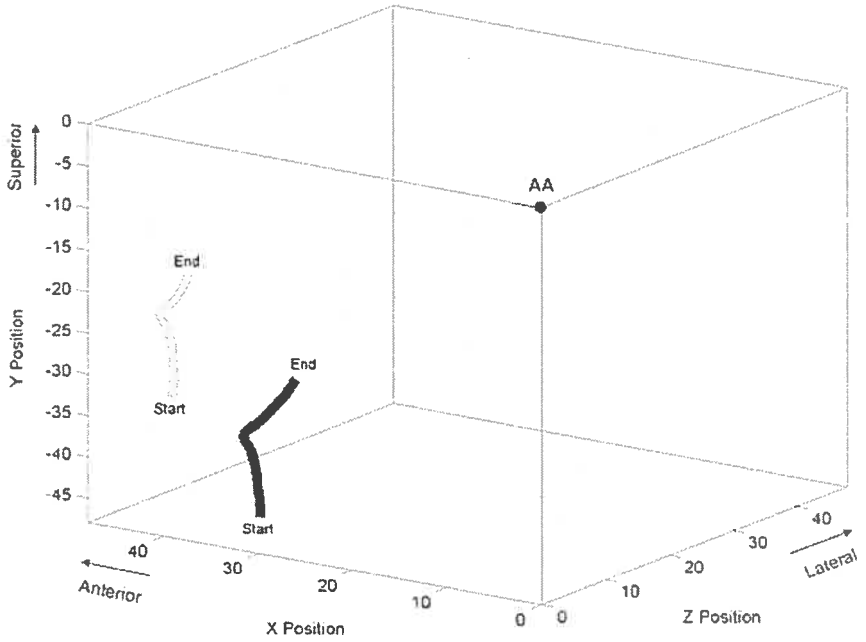

Figure 4.7: Mean 3D excursion of the geometric (grey line) and functional (black line) GHRC relative to the AA landmark for specimen #7.

The distance between the glenoid center and both GHRC (geometric and functional) was calculated in the resting position of the arm and at the maximum abduction (Figure 4.8). This distance was defined as the vectorial sum of the distances between the glenoid center and the GHRC in the sagittal and frontal plane. In the resting position, the distances averaged 11,1 ± 3,4 mm (range 7,3 to 18,2 mm) for the geometric GHRC and 15,4 ± 5,3 mm (range 9,4 to 26,5 mm) for the functional GHRC. In maximum abduction, the distance averaged 8,8 ± 5,3 mm (range 0,8 to 17,0 mm) for the geometric GHRC, and 11,1 ± 6,3 (range 0,6 to 20,7 mm) for the functional GHRC.

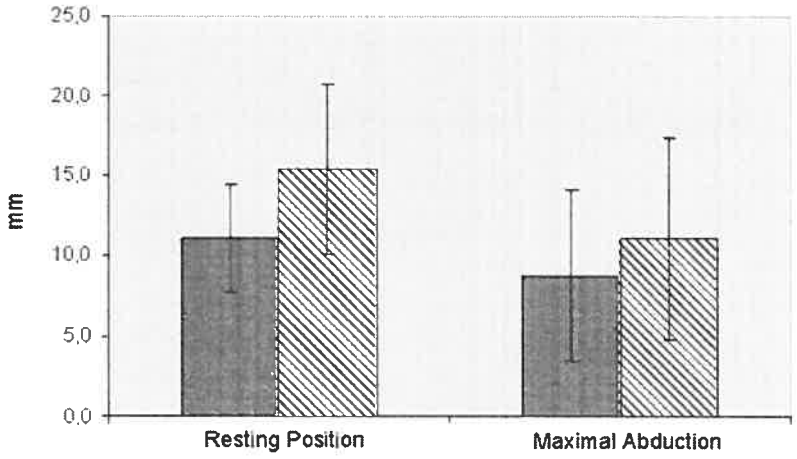

Figure 4.8: Mean distance between the glenoid center and the GHRC determined with the geometric (plain stick) and functional (lined stick) method.

4.5 Discussion

Our results show a difference between the position of the geometric and functional GHRC. These findings are in contradiction with Veeger (Veeger 2000), who found that the kinematic rotation center is not statistically different from the geometric center. This can probably be explained by the nature of the movement and the mathematical algorithm used to determine the functional GHRC. First, Veeger moved the humerus in three directions: abduction-adduction, flexion-extension, and internal-external rotation. The author did not execute a multiplan motion (i.e. circumduction motion). As Siston and Delp has shown, the smallest mean errors in determining the joint center occur with a circumduction motion pattern, while the largest errors occur with single-plan motion(Siston and Delp 2006). Therefore, Veeger's estimation of functional GHRC was not optimal because it omitted motion planes. Second, Veeger used the instantaneous helical axis (IHA) to calculate the functional GHRC, even if this method produces a large non-systematic error when estimating kinematic rotation center. Woltring (1990) has shown that the IHA calculations are extremely sensitive to errors when the rotation speed is small and the data noisy(Woltring 1990). Unlike Veeger, the pivoting algorithm was used in our study. According to Siston and Delp, the pivoting algorithm «is an accurate technique to locate the joint center which is minimally affected by reasonable limits of motion and the presence of noisy motion data».

The difference observed between the two GHRC in our study cannot be explained by the fact that the movement was carried out by an experimenter. In fact, the variability in GHRC localization was equivalent for both geometric and functional methods. For this reason, the way the circumduction movement was performed by the experimenter cannot be deemed to have had a significant impact.

It has long been assumed that the normal glenohumeral joint acts as a ball-and-socket joint with a fixed rotation center even though the rotator cuff is present but non-functional (Howell and Galinat 1989; Veeger 2000). «As long as there is a compressive force acting, the intact glenohumeral articulation would be expected to be stable and the humeral head will rotate on a more or less fixed center with little, if any excursion (Poppen and Walker 1976)». If we base ourselves on this affirmation, the GHRC should be localized at a point where its excursion is minimal during motion of the arm. According to Thompson (Thompson, Debski et al. 1996) and Keklar (Kelkar, Wang et al. 2001), the humeral head translation should be lower than 2 or 3 mm for a simulated abduction movement of at least 90°. In the same way, Wuelker and al. (Wuelker, Schmotzer et al. 1994) reported that the translation of the humeral head rotation center for a 30° abduction of the arm averaged 3,6mm ± 3,3mm superiorly and 0,0mm ± 2,3 anteriorly. Our results revealed that both GHRC moved between 7,1 ± 4,4 and 2,7 ± 1,8 mm during abduction of the arm. We reported larger displacement than previous published reports. This difference could be attributed to the initial position of the humeral head used for reporting the excursion. Unlike the present study, Thompson (Thompson, Debski et al. 1996) and Wuelker (Wuelker, Schmotzer et al. 1994) applied a small amount of upward forces (5N/N-m vs 23N ± 4,6N) on the arm at the beginning of each experiment. This force application consequently annihilates the effect of gravity and prevents the arm from subluxating inferiorly. Consequently, a smaller excursion was recorded. As to Keklar (Kelkar, Wang et al. 2001), « the position of the center of the humeral head at 90° was taken as a reference position for reporting humeral head translation. The position of 0° was not selected as a reference position because all joints had been vented and, as such, subluxated inferiorly at 0°».

The excursion of the geometric and functional GHRC recorded in the present study during abduction of the arm tends to demonstrate that the glenohumeral joint

does not behave only as ball and socket joint but in a more complex way. The glenohumeral joint does not have a fixed rotation point because rotation and translation occur simultaneously. Moreover, it was observed that excursion patterns differed for geometric and functional GHRC. During an abduction movement of the arm, the functional GHRC had a greater medial to lateral displacement than the geometric GHRC. However, the distance between both the geometric and functional GHRC stayed approximately the same with motion in the scapular plane.

Several studies have documented that the humeral head was precisely centered in the glenoid fossa. Poppen (Poppen and Walker 1976) and Howell (Howell and Galinat 1989) demonstrated in vitro that the center of the humeral head remained within 1mm of the center of the glenoid throughout the elevation of the arm. Biomechanical models of the shoulder joint were further developed based on this assumption. In the present study, the functional and geometric GHRC were not centered on the glenoid. The distance between the glenoid center and the geometric and functional GHRC varied between 11,1 ± 3,4 mm and 15,4 ± 5,3 mm respectively. The difference observed is probably due to the methodology used in the present study and the anatomy of the glenoid fossa. First, Poppen (1976) and Howell (1989) had used roentgenogram to calculate the distance between the geometric center of the humerus and the center of the glenoid. This type of imaging technique gives information only in one plane. Unlike them, the localisation of the GHRC relative to the glenoid center combined two planes (sagittal and frontal). If we consider only the frontal plane, a mean distance of 6,7 ± 4,5 mm was calculated between the geometric GHRC and the glenoid center. This higher value to the one observed by Poppen could be explained by the fact that the rotator cuff muscles were inactive. Poppen's research was done on living subjects while ours done made on cadaveric specimens. Second, anatomical studies have indicated that the articular surface of the glenoid fossa forms only one third to one quarter of the humeral head articular surface (Low and Reed 1996; Terry and Chopp 2000). According to Terry, the humeral head is in contact with only 25-30% of the glenoid cavity in all situations. Therefore, the small surface area of the glenoid does not enclose the humeral head. Being a joint with minimal bony constraint, the glenohumeral joint may consequently not be centered perfectly on the glenoid fossa in all three planes despite the presence of the labrum.

4.6 Conclusion

The GHRC is a very important landmark. It is a reference for the shoulder joint motion analysis and has to be localized precisely. In our study, the geometric GHRC and the functional GHRC were not localized at the same point and did not behave in the same way with motion. Because the humerus head rotated and translated on the glenoid, the assumption that the shoulder is a ball and socket joint is open to question. Consequently, future kinematics analysis must take into account the behaviour of geometric and functional GHRC. These findings could eventually be applied to conditions such as rotator cuff tear or cuff tear arthropathy. Therefore, it is possible to speculate that in the presence of a rotator cuff tear, geometric and functional GHRC move further apart because the stabilisation mechanism provided by the muscles is disturbed. Clinically, the dissociation between the geometric and functional GHRC could manifest itself in a loss of function, such as pseudoparalysis due to the rotator cuff rupture. In conclusion, this study demonstrates that three-dimensional analysis can be useful in providing additional information in comparison with two-dimensional analysis.

4.7 Acknowledgement

The authors would like to acknowledge CRSNG and FQRNT for funding. They are also grateful to Gerald Parent for his help.

Chapitre 5: Article II: Simplification of the ISB joint coordinate system to describe shoulder joint kinematics

A. Levasseur, P. Tétreault, J.A. de Guise, N. Nuño, N. Hagemeister

Article soumis à la revue «Clinical Biomechanics»

5.1 Abstract

The Joint Coordinate System (JCS) is a method used by the scientific community to describe joint motion. An important characteristic of JCS is to allow coherence between the performed movement, its mathematical representation and the clinical interpretation of its kinematics. In 2005, the International Society of Biomechanics (ISB) defined a JCS for the shoulder. To improve kinematics interpretation, the ISB suggested aligning the coordinate systems of the humerus and the scapula. The aim of this research project was to determine how aligning the JCS axes influenced the interpretation of shoulder joint kinematics. More precisely, we wanted to investigate if a mathematical alignment of the axis could facilitate the kinematic interpretation of a simple abduction movement without introducing cross-talk. An experiment was carried out on 8 shoulder cadaveric specimens. Elevation of the arm in the scapular plane (abduction) was recorded using an electromagnetic tracking device. Three dimensional (3D) angular displacements of the arm during elevation in the scapular plane were described using the ISB JCS, as well as a modified ISB JCS for which the axes were mathematically aligned. The results obtained revealed a difference in the interpretation of the starting angles between the ISB JCS and the aligned JCS. No difference was found in the interpretation of the angular range of motion. The aligned JCS provide a standardized starting angle of elevation that allowed an easier clinical interpretation of shoulder kinematics.

5.2 Introduction

In 2005, the International Society of Biomechanics (ISB) proposed Joint Coordinate System (JCS) for the shoulder (Figure 5.1) (Wu, van der Helm et al. 2005). These recommendations aimed at encouraging all authors to "(i) use the same set of bony landmarks, (ii) use identical local coordinate systems and (iii) and report motions according to this recommended standard" (Wu, van der Helm et al. 2005). This work has resulted in the standardization of shoulder joint motion description and provides better communication among researchers.

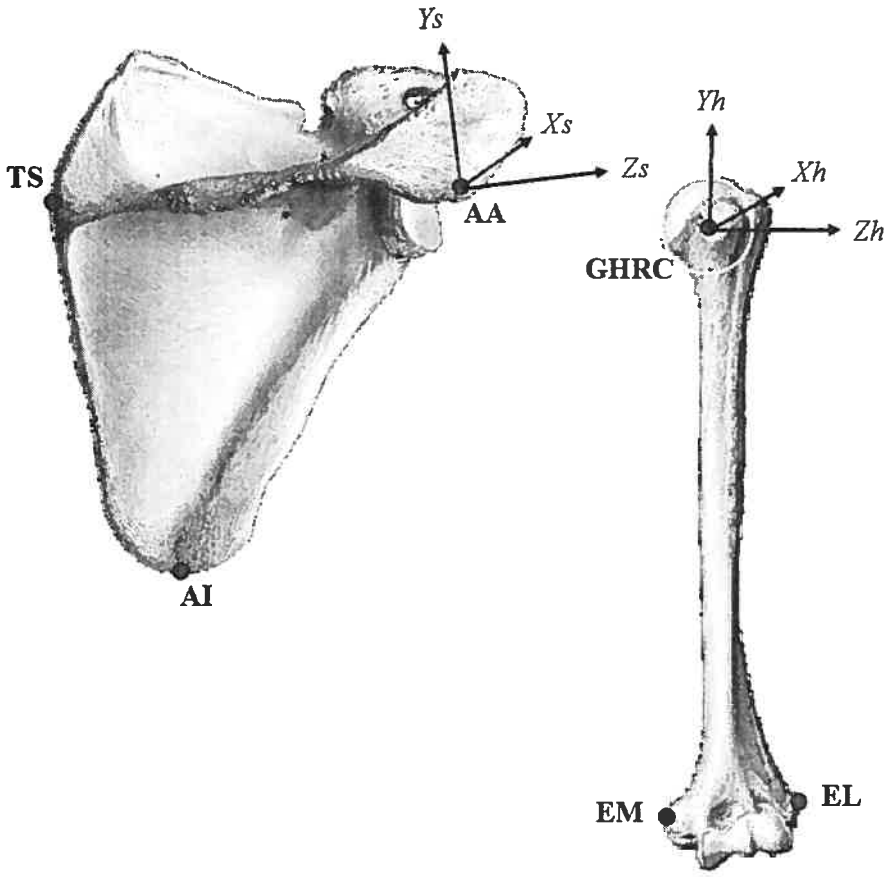

Bone	Anatomical Landmark	Description
Humerus (m)	GHRC	GlenoHumeral rotation center
	EL	Most caudal point on Lateral Epicondyle
	EM	Most caudal point on Medial Epicondyle
Scapula (r)	AC	Most dorsal point on the Acromioclavicular joint
	TS	Trigonum Spinae Scapulae, midpoint of triangular surface
	AI	on medial border of the scapula in line with the scapular
	AA	spine Angulus Interior, most caudal point of the scapula Angulus Acromialis, most latero-dorsal point of the scapula

Figure 5.1: Representation of the ISB JCS and description of the bony landmarks used to define the humerus and scapula coordinate systems

The ISB recommendations describe shoulder joint motion as a succession of three rotations of the humerus coordinate system relative to the scapula coordinate system (Y-X-Y in Euler angles). However, two major disadvantages arising from using three consecutive rotations about mobile axes have recently been reported (Senk and Cheze 2006). The first one is a «mathematical indetermination of angles

values close to 0° or 180°», which is commonly called gimbal lock (Senk and Cheze 2006). The second disadvantage concerns the sequence dependence, that is, that movement description is dependent on the order in which the rotation occurs (Grood and Suntay 1983; Skalli, Lavaste et al. 1995). This can produce inconsistencies in the kinematic representation of the movement performed, which can make motion analysis interpretation questionable. Nevertheless, the using of consecutive rotations still remains the principal tool to represent 3D angular displacement in clinical movement analysis (Senk and Cheze 2006).

Recently Šenk and Chèze demonstrated that movements described with the ISB JCS were not clinically interpretable because of the incidence of gimbal lock and of an inconsistency between the movement performed and its corresponding calculated range of motion. They showed that for an abduction movement of 90-100°, the calculated range of motion varies between 37,3° ± 8,9 to 97,8° ± 10,2. These findings were mainly attributed to the choice of the rotation sequence use. According to these authors, the best rotation sequence, that can be used to describe elevation in the scapular plane (abduction) is XZY, because it produced no incidence of gimbal lock. Nevertheless the interpretation of the described movement remains unsatisfactory in their view. It was adequate for elevation in the scapular plane, but not necessarily convenient for other movements. The impossibility of finding a correct clinical interpretation is due to the anatomical reference position of the scapula that is used as the origin for movement description (Senk and Cheze 2006).

For a clearer interpretation of shoulder joint motion, the ISB suggests starting by aligning the coordinate systems of the humerus and the scapula in relation to each other (Wu, van der Helm et al. 2005). To our mind, two different methods can be use to align both coordinate systems. The first method would be to position the upper arm so that both coordinate systems are initially aligned (anatomical alignment). The second would be to modify the JCS orientation without adjusting the upper arm position (mathematical alignment).

To the best of our knowledge, there has been no *in vitro* or *in vivo* study that compares the effect of JCS alignment on shoulder joint kinematics. Therefore, the aim of our study was to investigate, using cadaver shoulder specimens, how the

alignment of the axis influences the kinematic interpretation of a simple movement. To our mind, anatomical alignment has the disadvantage of forcing the arm in a non-anatomical position. A mathematical alignment would therefore seem to be a more interesting approach. Three-dimensional (3D) angular displacements of the arm during elevation in the scapular plane (abduction) will be described. Two joint coordinate systems will be used: ISB JCS, and the modified ISB JCS for which the axes have been mathematically aligned (aligned JCS). We tried to see if the JCS initial alignment could provide a clearer shoulder joint motion interpretation without introducing cross-talk.

5.2 **Methods**

5.2.1 **Specimen preparation**

Eight fresh-frozen shoulder cadaver specimens including entire arm were used (4 lefts and 4 rights, age range 59 to 87 years). The specimens were stored in a freezer at -20°C and thawed at room temperature for approximately 8 hours before the dissection. All soft tissues around the shoulder were removed except for the rotator cuff muscles, the capsule, the anterior and posterior deltoid. The forearm and the hand were left intact. The cadaver specimens did not show any musculoskeletal pathology as assessed by a senior orthopaedic surgeon. Two aluminium triangles were fastened with plastic screws on the scapula and on the humerus for calibration purpose. After dissection, the specimens were refrozen and then sent for CT scan. From the CT images, an individual 3D reconstruction was realized using a commercial software (SliceOmatic,Tomovision, Montréal, Canada).

5.2.2 Experimentation

A testing device made of an abduction guide and two mounting blocks was designed in our research laboratory to reproduce *in vitro* an abduction movement of the arm (Figure 5.2a). Prior to the experiment, the shoulder specimens were thawed again for a period of 12 hours at room temperature. To immobilize the relative motion between the humerus and the forearm, the elbow was fixed with a brass screw. The scapula was screwed to the main mounting block of the testing device in a manner to reproduce the anatomical position of the scapula (Figure 5.2b). The initial position of the arm was consequently perpendicular to the ground, in 0°

abduction and 0° horizontal abduction. It hang freely between the guiding boards, to ensure abduction in the plane YZ of the scapula. The middle deltoid was replaced by a strip of non-elastic fabric to simulate its function as main abductor of the arm (Figure 5.2b). One extremity of the fabric strip was fixed to the deltoid tuberosity and the other to a pulling mechanism (Figure 5.2a). The pulling mechanism (Figure 5.2c) consisted of an electric cylinder (NV-D Series, Industrial Device Coorporation, Rockford, USA) which was used to simulate a continuous abduction movement of the arm at constant speed (≈10°/s). To prevent slipping of the fabric strip off the acromion during traction of the electric cylinder, a guiding device was attached on top of the scapula (Figure 5.2d). This device also helped reproduce the line of action of the middle deltoid muscle.

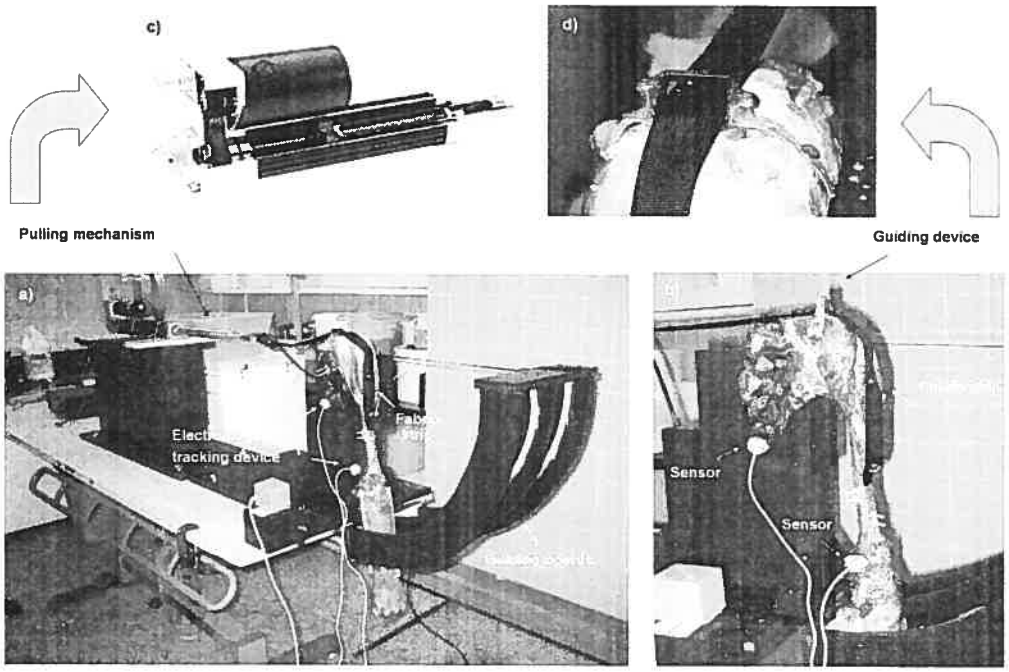

Figure 5.2: (a) *In vitro* testing device: (b) position of the scapula on the main mounting block of the testing device; (c) electric cylinder; (d) guiding device

3D shoulder joint motion was recorded using an electromagnetic tracking device (Fastrak, Polhemus, Colchester, USA) (Figure 5.2a). The accuracy of the system is 1mm for linear displacement and 0,1° for angular displacement. Sensors were screwed on plastic plates which were directly fixed on the scapula and humerus (Figure 5.2b). The sensor on the scapula served as a control for possible movement

of the scapula on the testing device in spite of it being rigidly fastened. A personal computer with custom-design software recorded in real time the 3D displacement of the arm at 60 Hz.

The experimental session was divided in 5 stages (Figure 5.3). Prior to data acquisition, a calibration procedure was realized. It consisted in digitalizing the extremity of both triangles fastened on the scapula and the humerus using a Fastrak pointer. This procedure allowed to establish a transformation matrix between the motion of the specimen and the individual 3D reconstruction. The ISB JCS and the aligned JCS were then defined.

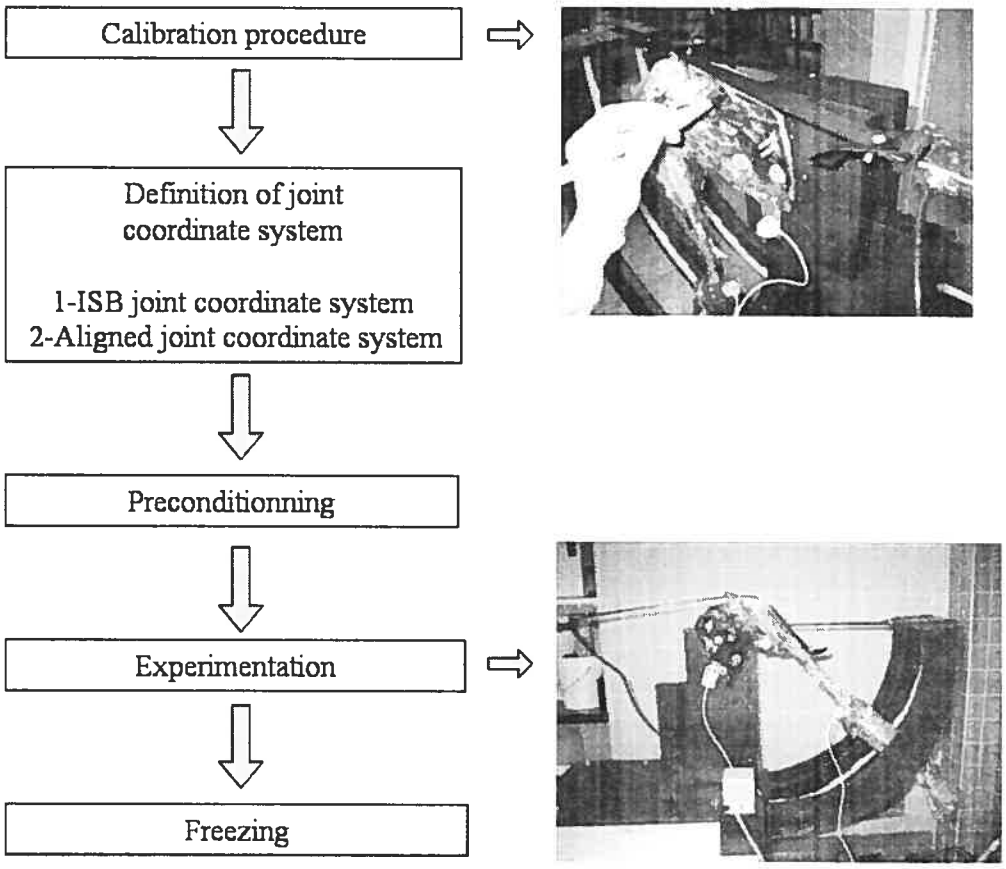

Figure 5.3: Summary of the experimental procedure

5.2.3 ISB JCS

The ISB recommendation regarding shoulder JCS definition is based on scapular and humeral anatomical bony landmarks (table in Figure 5.1). It requires the

definition of two local coordinate systems: one for the scapula (reference coordinate system) and one for the humerus (moving coordinate system) (Figure 5.4a). The purpose of anatomical axes is to allow rotations about axes that can be anatomically meaningful (Wu, van der Helm et al. 2005).

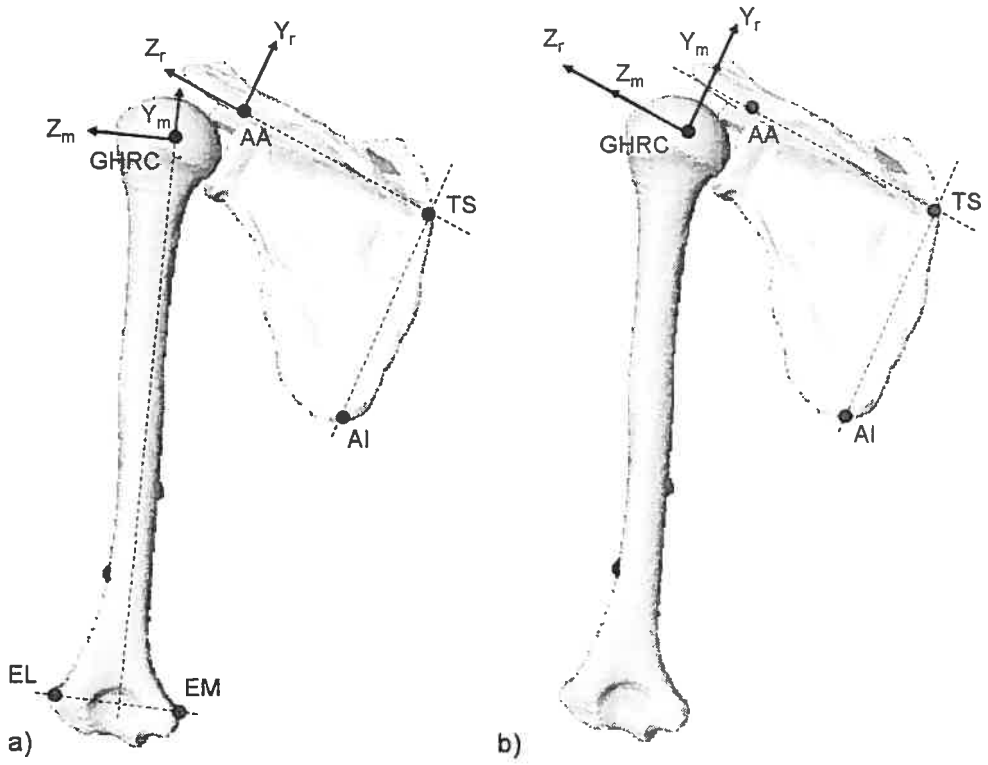

Figure 5.4: Definition of (a) the ISB joint coordinate system and (b) the aligned joint coordinate system where 'r' and 'm' denotes reference JCS and moving JCS respectively.

The reference coordinate system ($_r$) origin is positioned at the angulus acromialus of the scapula (AA). Its orientation is defined according to scapular bony landmarks listed in the table in Figure 5.1. The Z_r axis is defined as the line connecting TS and AA, pointing towards AA. The X_r axis is defined as the line perpendicular to the plane formed by AI, AA and TS, pointing forward. The Y_r axis is the common line perpendicular to X_r and Z_r and pointing upward (Figure 5.4a).

The moving coordinate system ($_m$) origin is positioned at the glenohumeral rotation center (GHRC) (Figure 5.4a). Its orientation is defined according to humeral bony landmarks listed in the table in Figure 5.1. The GHRC is the only humeral bony landmark that must be estimated. According to the ISB recommendation, the choice of the method used to estimate the GHRC is left to the discretion of the author (Wu, van der Helm et al. 2005). In the present study, the GHRC corresponds to the center of a sphere fitted by a least square method to the articular surface of the humeral head (Helm, Veeger et al. 1992). Once the localisation of GHRC has been estimated, the humerus coordinate system can be defined. The Y_m axis is defined as the line connecting GHRC and the midpoint of EL and EM pointing to GHRC. The X_m axis is defined as the line perpendicular to the plane formed by EL, EM and GHRC and is directed forward. The Z_m axis is the common line perpendicular to Y_m and X_m pointing to EL.

The motion of the moving coordinate system is described relative to the reference coordinate system. The transformation matrix between the reference coordinate system ($_{Rcs}$) and the moving reference system ($_{Mcs}$) is calculated as follows.

$$T_{Rcs}^{Mcs} = \left[T_G^{S1} * T_{S1}^{Rcs}\right]^{-1} * \left[T_G^{S2} * T_{S2}^{Mcs}\right] \qquad \text{(Equation 1)}$$

As shown in Figure 5.5, T_G^{S1} defines the transformation matrix between the global frame ($_G$) and the sensor on the scapula ($_{S1}$), T_{S1}^{Rcs} the transformation matrix between the sensor on the scapula and the reference JCS, T_G^{S2} the transformation matrix between the global frame and the sensor on the humerus ($_{S2}$) and T_{S2}^{Mcs} the transformation matrix between the sensor on the humerus and the moving JCS respectively. Rotations were described using Euler angles. The rotation sequence XZY from Šenk and Chèze (Senk and Cheze 2006) was used because they observed no incidence of gimbal lock when describing elevation in the scapular plane.

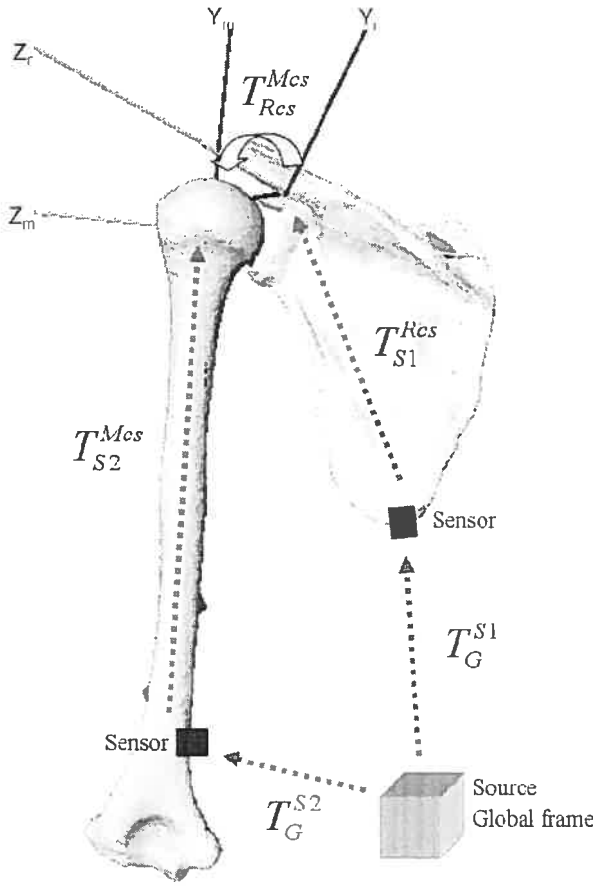

Figure 5.5: Representation of the transformation matrix used to express the motion of the moving coordinate system relatively to the reference coordinate system using the ISB JCS.

5.2.4 Aligned JCS

The aligned JCS requires the definition of two local coordinate systems: one for the scapula (reference coordinate system) and one for the humerus (moving coordinate system) (Figure 5.4b), based on the same bony landmarks that were defined previously (table in Figure 5.1).

The reference coordinate system ($_r$) orientation is defined according to scapular bony landmarks listed in the table of figure 1, but is positioned at the GHRC on the humerus. As previously mentioned, the GHRC is estimated as the center of a sphere fitted by a least square method to the articular surface of the humeral head (Helm, Veeger et al. 1992). The Z_r axis is defined as the line connecting TS and AA.

pointing towards AA. The X_r axis is defined as the line perpendicular to the plane formed by AI, AA and TS, pointing forward. The Y_r axis is the common line perpendicular to X_r and Z_r and pointing upward (Figure 5.4b).

The moving coordinate system ($_m$) origin is positioned at the GHRC (Figure 5.4B). Instead of being defined with the humerus bony landmark, its orientation is mathematically changed to make it parallel and coincident to the reference coordinate system when the arm is in resting position (i.e. 0° abduction, horizontal abduction and rotation). The moving coordinate system orientation is consequently defined according to scapular bony landmarks as referred by the table in Figure 1. The Z_m axis is defined as the line connecting TS and AA, pointing towards AA. The X_m axis is defined as the line perpendicular to the plane formed by AI, AA and TS, pointing forward. The Y_m axis is the common line perpendicular to X_m and Z_m and pointing upward.

Similar to the ISB JCS, the motion of the moving coordinate systems is described relatively to the reference coordinate systems as previously described by the equation 1. Rotations are described using Euler angles and the rotation sequence XZY from Šenk and Chèze was used (Senk and Cheze 2006).

Once both JCS were defined, 25 movements of abduction through the maximum range of motion were carried out with the pulling mechanism to condition the specimen (Debski, McMahon et al. 1995; Thompson, Debski et al. 1996; Parsons, Apreleva et al. 2002). After preconditionning, 10 abduction movements of maximum range of motion were completed using the pulling mechanism and recorded. Each trial lasted 10 seconds. During experimentation, the specimens were kept moist with saline solution. Afterwards, they were returned to the freezer at -20°C.

The initial position of the arm was defined as the angle between the moving and reference JCS around the 3 axes when the arm was at rest (Figure 5.6a). Movement range of motion in the three planes was defined as the angle difference between the final and the initial position of the arm (Figure 5.6b).

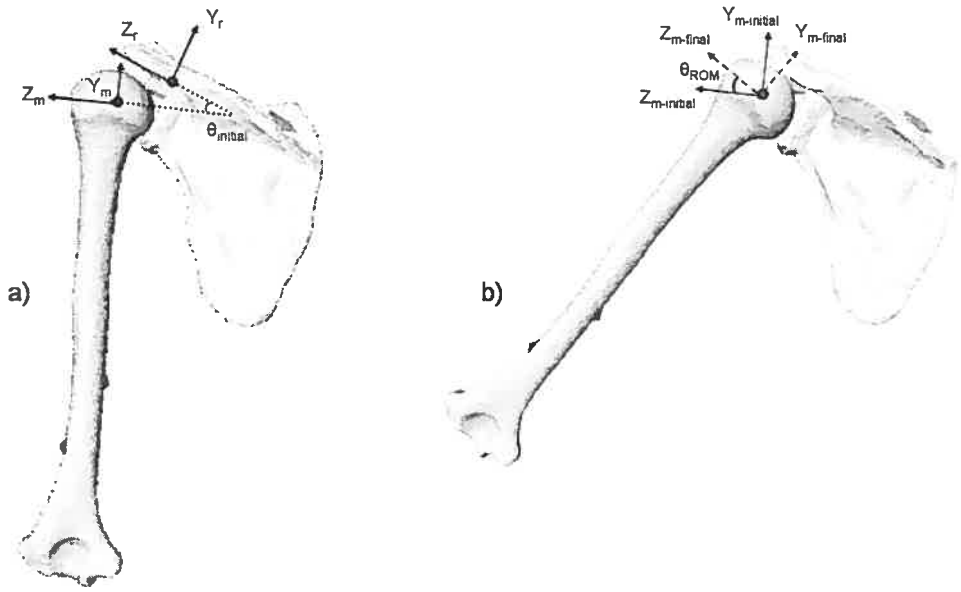

Figure 5.6: Representation of (a) the initial abduction angle when the arm is at rest and (b) the abduction range of motion where 'r' and 'm' denotes reference JCS and moving JCS respectively.

5.3 Statistical analysis

A two-way ANOVA for repeated measurements was used to determine whether a difference could be found between the abduction range of motion described using the ISB JCS and that of the aligned JCS. The same statistical test was performed for the horizontal abduction and the rotation range of motion. A two-way ANOVA for repeated measurements was also used to determine whether there was a difference between the initial position of the arm around the 3 axes described using the ISB JCS and the aligned JCS. Statistical significance was set at $\rho < 0.01$. All analyses were performed using the SPSS software.

5.4 Results

Table 5.1 presents the mean and standard deviations for the range of motion and initial position of the arm obtained during 10 trials involving 8 specimens. It is interesting to note that no discontinuity (gimbal lock) in the kinematics curves representation was reported for neither ISB JCS nor aligned JCS. This observation was valid for all trials and all specimens.

Table 5.1: Mean range of motion (SD) and mean initial position of the arm (SD) in degrees computed with the ISB JCS and the aligned JCS.

		ISB JCS	Aligned JCS
		° ± SD	° ± SD
Range of motion	*Abduction*	36,4 ± 6,7	36,7 ± 6,5
	Horizontal Flexion	8,5 ± 7,6	9,6 ± 7,7
	Rotation$_{int/ext}$	10,0 ± 6,6	8,6 ± 7,0
Initial position	*Abduction*	14,0 ± 7,9	0,2 ± 0,2
	Horizontal Flexion	18,1 ± 10,6	0,1 ± 0,1
	Rotation$_{int/ext}$	3,5 ± 2,6	0,1 ± 0,0

5.4.1 Range of motion

The abduction range of motion measured on the 8 specimens varied between 28,1° ± 0,2 to 45,4° ± 0,3 for the ISB JCS and between 28,8° ± 0,7 to 44,9 ± 0,3 for the aligned JCS. For horizontal abduction (movement parallel to the ground), it varied between 1,4° ± 0,4 to 24,0° ± 0,5 for the ISB JCS and between 1,4° ± 0,4 to 25,2° ± 0,5 for the aligned JCS. As for rotation, range of motion varied between 2,8° ± 0,0 to 24,2° ± 0,51 for the ISB JCS and between 0,8° ± 0,0 to 24,2° ± 0,1 for the aligned JCS.

For abduction and horizontal abduction, there was no statistically significant difference between the magnitude ranges of motion computed with ISB JCS and aligned JCS respectively. Rotation was the only range of motion when ISB JCS and aligned JCS showed a statistically significant difference (ρ =0,002). The mean difference between ISB JCS and aligned JCS was 1,4 ± 0,8°.

5.4.2 Initial position of the arm

For abduction, the initial position of the arm varied between 5,6° ± 0,0 to 28,8° ± 0,2 for the ISB JCS and between 0,0° ± 0,0 to 0,6° ± 0,4 for the aligned JCS. For horizontal abduction, it varied between 0,1° ± 0,1 to 30,8° ± 0,0 for the ISB JCS and between 0,0° ± 0,0 to 0,3° ± 0,1 for the aligned JCS. As for rotation, the initial

position varied between 0,1° ± 0,1 to 8,1° ± 0,0 for ISB JCS and between 0,0° ± 0,0 to 0,1° ± 0,1 for aligned JCS.

For abduction and horizontal abduction, there was a statistically significant difference between the initial positions of the arm computed with ISB JCS and aligned JCS. For rotation, there was no statistically significant difference between ISB JCS and aligned JCS. The mean difference between the initial positions computed with the ISB JCS and aligned JCS was 3.4 ± 2.6°.

5.5 Discussion

Cross-talk effect (coupled motion) is a concern when describing joint motion. When using Euler angles, abduction can cross-talked into horizontal abduction, and into rotation. It usually results from an ill-defined JCS. No cross-talk effect was reported for alinged JCS since no significant difference was observed between the range of motion computed with the ISB JCS and the aligned JCS.

We did not expect to find any difference between the magnitude ranges of motion calculated with ISB JCS and aligned JCS because motion description is "the characterization of how the relative position of two bodies changes with time" (Grood and Suntay 1983). A statistical difference was observed only for rotation but it was not considered significant from a clinical point of view (1.4°).

The description of the initial position of the arm was influenced by the JCS used. It must be noted that care was taken at the beginning of the experiment, to position the arm perpendicular to the ground, so that its resting position was at 0° of abduction and horizontal abduction. However, with the ISB JCS, interpreting the initial position of the arm led to the conclusion that most specimens were in negative abduction, positive or negative horizontal abduction and positive or negative rotation. In addition, when using ISB JCS, the initial position of the arm around the 3 axes varied from one specimen to the next. This inter-specimen variability complicated the task of comparing specimens.

With the aligned JCS, interpretation of the initial position of the arm was facilitated because of its standardization. At rest, the arm was in fact at 0° of

abduction, horizontal abduction and rotation, which is more meaningful from a clinical point of view. Furthermore, the alignment of the JCS was found to reduce inter-specimen variability and consequently facilitate comparisons between specimens. However, before aligning the JCS, it should be ensured that the arm is properly positioned.

We expected to find a difference between the initial position of the arm calculated with the ISB JCS and the aligned JCS, because the initial orientation of the JCS was voluntarily modified in a manner to standardize it at 0° of abduction, horizontal abduction and rotation. The absence of any significant difference for rotation could be explained by two specimens for which the difference was lower than 1.1°. This small difference between the initial position of the ISB JCS and the aligned JCS can be attributed to the position of the scapula, which made the JCS Y-axes already aligned.

Our finding showed that ISB JCS and aligned JCS did not cause any incidence of gimbal lock. No discontinuity in the kinematic curves was reported for any of the trials for all specimens. With its greater sample size (8 specimens instead of 5), our study confirms Šenk and Chèze's findings (Senk and Cheze 2006). The latter did not observe any gimbal lock when using the rotation sequence XZY to compute elevation of the arm in the scapular plane. The skin artefact which was identified as a possible experimental source of error by these authors can be refuted, since similar results were obtained with the use of markers directly fastened on the bones. Thus, the XZY rotation sequence is an appropriate means of describing elevation of the arm in the scapular plane.

In our *in vitro* study, the scapula was positioned on the testing device in such a way that it reproduced its *in vivo* anatomical orientation in a resting position (Culham and Peat 1993; Della Vallee, Rokito et al. 2001). It was therefore slightly rotated in the coronal plane, which did not necessarily make the two coordinate systems parallel to each other. To align the JCS without changing bone orientation, the idea of using a mathematical approach thus seemed interesting. However, it has the disadvantage of making the moving coordinate axis no longer coincident with the anatomical longitudinal axis of the humerus.

It is difficult to compare our findings with those of previous studies because of the recent publication of the ISB JCS. To the best of our knowledge, Šenk and Chèze were the first to report problems related to using ISB JCS(Senk and Cheze 2006). Mathematical alignment of the JCS axes appeared to be a way of enhancing standardization of shoulder joint motion description so that it would foster better communication among researchers.

The use of the aligned JCS could demonstrate major benefits for future kinematics analysis. Since it is built on scapula bony landmarks only, it could eventually be used to analyze the shoulder joint motion of the humerus amputed at the level of the epicondyle or of the humerus with deformities (i.e. axial torsion of the humerus causing misalignment of the epicondyle). Moreover, using only scapula bony landmarks decreases the quantity of landmarks that have to be localized. Indeed, "the in vivo localisation of external anatomic landmarks is known to be difficult and subjective" (Marin, Mannel et al. 2003). Precision errors related to anatomical landmark localisation may lead to mislocation and misorientation of the JCS that would ultimately affect kinematics motion analysis.

The limitations of this study can mainly be related to the testing device used. Firstly, this device was designed to simulate the elevation of the arm in the scapular plane only. Therefore, the influence of axis alignment on other movements such as flexion, extension or circumduction could not be evaluated. Secondly, our testing device was designed to simulate only the action of the middle deltoid. Constraints for the horizontal abduction had to be imposed (guiding board) to ensure elevation of the arm in the scapular plane. Nevertheless, it is important to mention that this device is the first one to simulate a continuous motion of the arm.

5.6 Conclusion

The JCS definition recommended by the ISB is a major improvement in shoulder joint motion analysis. It encourages researchers to use standards that stimulate communication and discussion in the biomechanical field. To avoid representation and interpretation problems, the ISB suggests aligning both JCS. We

have investigated here the effect of axis alignment on shoulder kinematics. We proposed a mathematical approach to align the JCS and demonstrated that the alignment of the JCS axis can provide a clearer shoulder joint motion interpretation without introducing cross-talk. Moreover, the recorded range of motion did not differ with the aligned JCS. The latter provided more relevant information on the initial position of the arm. By starting at 0°, it reduced inter-specimen variability and made interpretation of kinematics easier. Future kinematics studies must be realized to determine if the aligned JCS can prove useful for the analysis of more complex movements such as circumduction.

5.7 Acknowledgement

The authors would like to acknowledge the financial support of NSERC and FQRNT. They are also grateful to Gerald Parent for his help.

Chapitre 6: Article III: Determination of pathological shoulder biomechanics caused by simulated rotator cuff tear in an *in vitro* system

P. Tétreault, A. Levasseur, J.A. de Guise, N. Nuño, N. Hagemeister

Article soumis au journal «Shoulder and Elbow Surgery»

6.1 Abstract

The clinical presentation of a massive rotator cuff tear of the shoulder has a wide spectrum of symptoms and signs, ranging from minimal limitation in range of movement to full pseudoparalysis. Functional recovery of a pseudoparalytic shoulder after treatment by arthroplasty remains unpredictable and incomplete. Although a better understanding of how normal shoulder biomechanics is altered by a massive rotator cuff tear may lead to better prosthetic design, few *in vitro* studies have specifically examined this. Therefore, we used an *in vitro* shoulder abduction model to study the pathologic shoulder kinematics caused by a simulated massive rotator cuff tear in 8 cadaver shoulders. We simulated elevation of the arm in the plane of the scapula by replacing the middle deltoid with a standardized pulling mechanism. After ten cycles of elevation with the rotator cuff intact, we surgically created a massive cuff tear and repeated the cycles of arm elevation. The 3D displacement of the glenohumeral rotation center (GHRC) and the force required for arm elevation were recorded. We found a significant increase in the lateral and superior displacement of the GHRC in shoulders with a massive cuff tear. We also found a significant increase in the force required for the first 30 degrees of arm elevation in these specimens. We conclude that alteration of morphologic features about the glenohumeral joint can have a significant impact on shoulder kinematics. Further studies may help identify parameters to guide novel prosthetic design in the treatment of cuff tear arthropathy.

Key words: Rotator cuff tear, shoulder kinematics, cuff tear arthropathy, motion analysis

6.2 Introduction

Cuff tear arthropathy (CTA) is a debilitating condition of the shoulder causing destruction of the glenohumeral joint and inability to elevate the arm, or pseudoparalysis. The current standard treatment for CTA is a shoulder hemiarthroplasty. The pain relief with this treatment is significant, but the gain in function is unpredictable and incomplete (Neer, Craig et al. 1983; Arntz, Jackins et al. 1993; Williams and Rockwood 1996; Field, Dines et al. 1997; Zeman, Arcand et al. 1998; Zuckerman, Scott et al. 2000; Baumgarten, Lashgari et al. 2004). Attempts have been made to design a shoulder prosthesis which would be equally good at relieving the pain of CTA but also better in restoring shoulder function in these patients (Sirveaux, Favard et al. 2004; Visotsky, Basamania et al. 2004; Boileau, Watkinson et al. 2005). However, none of the currently available prostheses has been proven to achieve these goals without additional complications.

A better understanding of the normal biomechanics of shoulder movement and the role of the rotator cuff muscles, as well as how this is altered in CTA is essential to understand how pseudoparalysis develops, and to design better shoulder prostheses for the treatment of this condition.

Several studies have used *in vitro* models to investigate the function of the rotator cuff (Loehr, Helmig et al. 1994; Sharkey and Marder 1995; Wuelker, Wirth et al. 1995; Karduna, Williams et al. 1996; Halder, Zhao et al. 2001). Debski and colleagues developed a complex, dynamic *in vitro* testing device to analyze the glenohumeral motion on a full cadaver arm (Debski, McMahon et al. 1995), and Thompson used that device to simulate rotator cuff tendon paralysis and various sizes of cuff tears (Thompson, Debski et al. 1996). They found that the joint could maintain ball-and–socket kinematics as long as the infraspinatus remained functional. With a massive cuff tear in their model, the maximal abduction is 25 degrees despite a threefold increase in middle deltoid force.

Interestingly, not all patients with a massive cuff tear ultimately develop a painful pseudoparalytic shoulder. Several authors have described cases where the affected shoulder had minimal pain and near normal range of motion, despite the presence of a massive cuff tear (Burkhart 1992; Burkhart, Esch et al. 1993; Burkhart, Nottage et al. 1994; Yamaguchi, Sher et al. 2000; Schibany, Zehetgruber et al. 2004). Burkhart noted that a ridge of fibrous residual cuff could act as a fulcrum of the

humeral head and allow the deltoid muscle to elevate the arm(Burkhart 1992). Inman has added the concept of force couples to this hypothesis (Inman, Saunders et al. 1996). This concept implies that elevation of the arm is possible as long as the cuff forces, anterior and posterior to the rotation center, are balanced and provide sufficient inferior compression.

To our knowledge, no studies have determined which factors may be linked to the development of pseudoparalysis, nor has this clinical finding been specifically addressed with an *in vitro* model to date. We hypothesize that the position of the glenohumeral rotation center, the morphology of the proximal humerus, the length of the acromion, the deltoid lever arm, and the magnitude of proximal humeral migration may all have a role to play in the appearance of pseudoparalysis in CTA. In this paper, we establish a simple, *in vitro,* dynamic model of shoulder pseudoparalysis, to further investigate the pathological alterations in shoulder biomechanics due to massive rotator cuff tear. A better understanding of how normal shoulder kinematics is altered in CTA may help to identify morphological features of pseudoparalytic shoulders that can be altered to improve current shoulder prosthetic design for CTA treatment.

6.3 Method

6.3.1 Specimen preparation

Eight fresh-frozen shoulder cadaver specimens, including the entire arm were used (4 lefts and 4 rights, age range 59 to 87 years). The specimens were stored in a freezer at -20°C and thawed at room temperature for approximately 8 hours before the dissection. All soft tissues around the shoulder were removed except for the rotator cuff muscles, the shoulder capsule and the anterior and posterior deltoid muscle. The forearm and hand were left intact. The cadaver specimens did not show any musculoskeletal pathology as assessed by a senior orthopaedic surgeon. Two aluminum triangles were fastened with plastic screws to the scapula and to the humerus for calibration purposes. After dissection, the specimens were refrozen and then sent for CT scanning. From the CT images, an individual 3D reconstruction of the shoulder joint was made using a commercial software (SliceOmatic,Tomovision, Montréal, Canada).

6.3.2 Experimentation

A testing device composed of an abduction guide and two mounting blocks was designed in our laboratory to reproduce the abduction movement of the arm *in vitro* (Figure 6.2A). Prior to the experiment, the shoulder specimens were thawed again for a period of 12 hours at room temperature. To eliminate motion between the humerus and the forearm, the elbow was immobilized with a brass screw. The scapula was fixed to the main mounting block of the testing device in anatomical position (Figure 6.2B). Therefore, the initial position of the arm in this model was perpendicular to the ground, in 0° of abduction, hanging freely between the guiding boards. The middle deltoid was replaced by a strip of fabric to simulate its function as the main abductor of the arm (Figure 6.2B). One extremity of the fabric strip was fixed to the deltoid tuberosity and the other to a pulling mechanism (Figure 6.2A). The pulling mechanism (Figure 6.2C) consisted of an electrical cylinder (NV-D Series, Industrial Device Coorporation, Rockford, USA) which was used to simulate a continuous abduction movement of the arm at constant speed (≈10°/s). To prevent slipping of the fabric strip off the acromion during traction of the electric cylinder, a guiding device was attached on top of the scapula (Figure 6.2D). This device also

helped to reproduce the line of action of the middle deltoid muscle. The force was recorded with a tensiometer in Newtons.

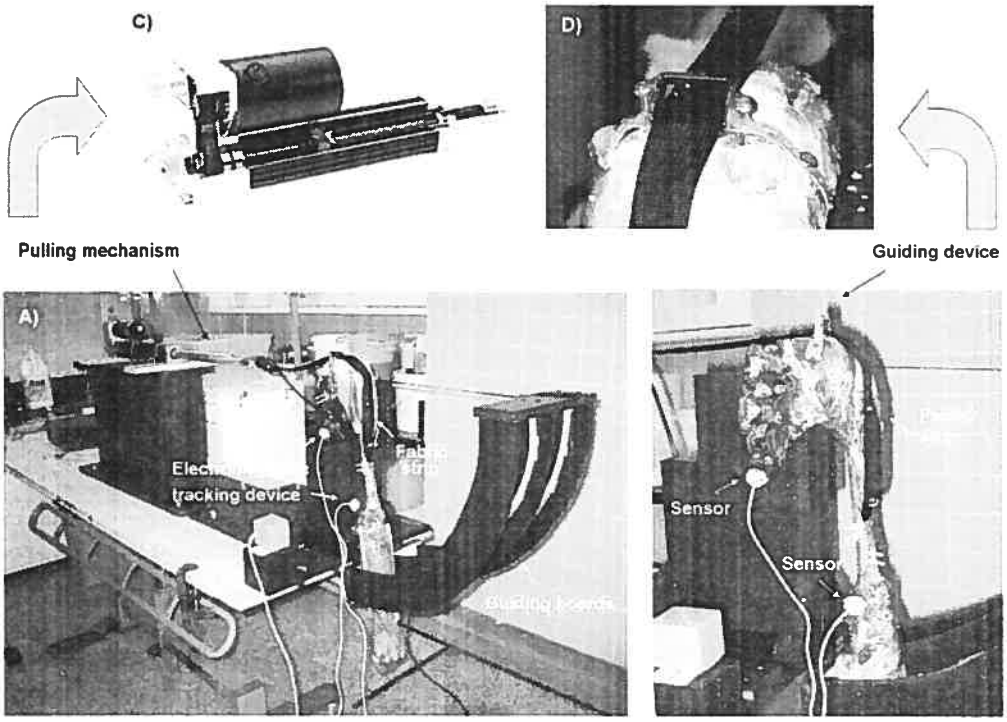

Figure 6.1: A- *In vitro* testing device: B- position of the scapula on the main mounting block of the testing device; C- electric cylinder; D- guiding device.

Three dimensional shoulder joint motion was recorded using an electromagnetic tracking device (Fastrak, Polhemus, Colchester, USA) (Figure 6.2A). The accuracy of the system is 1mm for linear displacement and 0.1° for angular displacement. Sensors were screwed on plastic plates which were directly fixed on the scapula and humerus (Figure 6.2B). The sensor on the scapula served as a control for possible movement of the scapula on the testing device in spite of it being rigidly fastened. A computer with custom-designed software recorded in real time the 3-D displacement of the arm at 60 Hz.

The experimental session was divided into 5 stages (Figure 6.3). Prior to data acquisition, a calibration procedure was carried out. It consisted of digitalizing the tips of the calibration triangles fastened onto the scapula and the humerus using a

Fastrak pointer. This procedure allowed us to establish a transformation matrix between the actual motion of the specimen and the corresponding 3-D reconstruction, generated from CT scanning of the specimen as described above. For kinematic analysis, we used an aligned joint coordinate system (AJCS), which has both the reference axis and the moving axis aligned at the starting position. We have previously shown that alignment of the axis over the glenohumeral rotation center (GHRC) greatly facilitates the interpretation of the data and graphics (Levasseur, Tétreault et al. 2006).

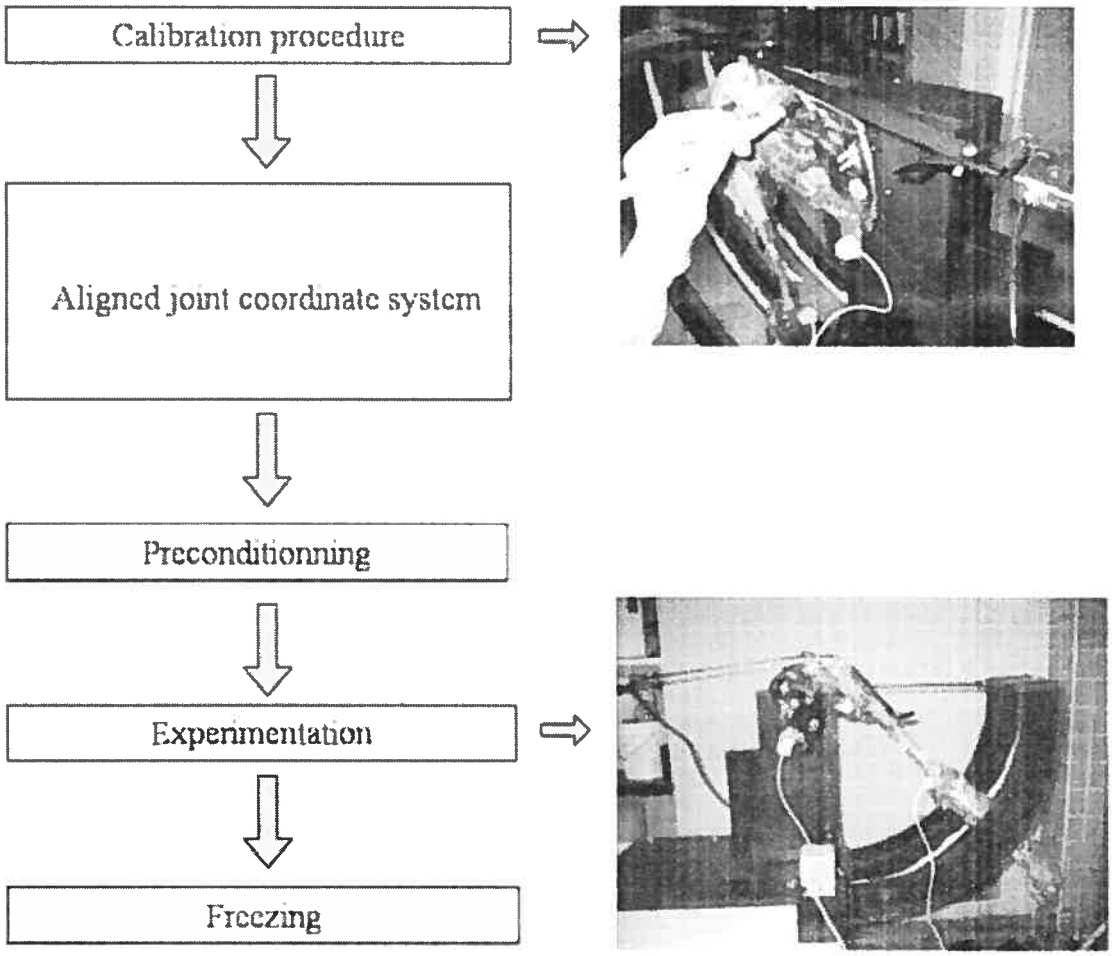

Figure 6.2: Summary of the experimental procedure.

For each specimen, we used a 3D reconstruction for estimation of the geometric GHRC. We used the software called Polyworks (InnovMetric, Canada) for a point cloud selection (Figure 6.4). The selection was made manually three times by one person. Using the least square method, a sphere was fitted to the data of the point

cloud (Figure 6.4)(Meskers, van der Helm et al. 1998). The geometric GHRC corresponded to the center of this sphere.

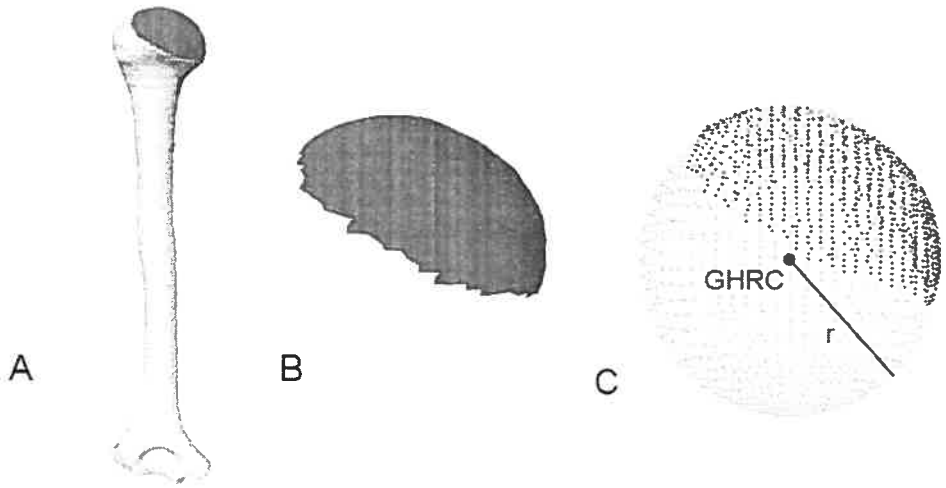

Figure 6.3: A- Selection of point cloud on the 3D reconstruction of the humeral head; B- point cloud; C- sphere estimated by a least square method.

Thereafter, 25 movements of abduction through the maximum range of motion were carried out with the pulling mechanism to condition the specimen (Debski, McMahon et al. 1995; Thompson, Debski et al. 1996; Parsons, Apreleva et al. 2002). Following this preconditioning, 10 abduction cycles through the maximal range of motion were completed using the pulling mechanism and recorded. Each trial lasted 10 seconds. During experimentation, the specimens were kept moist with 0.9% NaCl saline solution. We then selectively cut the tendon of the supraspinatus, the upper half of the infraspinatus tendon, and the upper half of the subscapularis tendon including the biceps tendon and repeated a cycle of 10 repetitive elevations. Afterwards, the specimen was returned to the freezer at -20°C.

6.4 Statistical analysis

A two-tailed paired t-test for repeated measurements was used to determine whether a difference could be found between the displacement the geometric GHRC during abduction with and without an intact cuff tear. A two tailed paired t-test was used to identify any significant difference in the force required for elevation of the

arm with and without an intact cuff. Statistical significance was set at $\rho < 0.05$. All analyses were performed using the SPSS software.

6.5 Results

6.5.1 Anterior and posterior displacements of the GHRC (*x*-axis) after elevation of the arm, with and without an intact rotator cuff.

Table 6.1 shows the values obtained for the displacement of the geometric GHRC on the *x*-axis before and after a massive rotator cuff tear. A positive value represents an anterior displacement and a negative value represents a posterior displacement relative to the initial starting position, which is set to 0. A displacement is measured in millimeters.

Table 6.1: Average anterior and posterior displacement (mm) of the GHRC (x-axis) with and without an intact rotator cuff.

Specimen	Geometric GHRC with cuff intact (mm)	Standard Deviation (mm)	Geometric GHRC with cuff tear (mm)	Standard Deviation (mm)
1	0	0	1	0
2	2	0	4	0
3	1	0	-1	0
4	-2	0	-4	0
5	6	0	4	0
6	-5	1	-12	0
7	-2	0	-3	0
8	-3	1	-3	1
Mean	0	4	-2	5

* for p value < 0.05

Each value in the table represents the average displacement of the GHRC after 10 repetitions of arm elevation. On average, elevation of the arm with the rotator cuff intact caused minimal anterior/posterior displacement of the GHRC (mean of 0 mm). A massive cuff tear did not significantly cause a greater displacement of the GHRC on the anteroposterior *x*-axis (p=0.143). For most

specimens (5 specimens out of 8), a rotator cuff tear caused the GHRC to displace posteriorly, but not significantly.

6.5.2 Medial and lateral displacement of the GHRC (*z*-axis) after elevation of the arm, with and without an intact rotator cuff.

Table 6.2 shows the values obtained for the displacement of the geometric GHRC on the *z*-axis before and after a massive rotator cuff tear. A positive value represents a lateral displacement and a negative value represents a medial displacement relative to the initial starting position, which is set to 0. A displacement is measured in mm.

Table 6.2: Average medial and lateral displacement (mm) of the GHRC (*z*-axis) with and without an intact rotator cuff.

Specimen	Geometric GHRC with cuff intact (mm)	Standard Deviation (mm)	Geometric GHRC with cuff tear (mm)	Standard Deviation (mm)
1	0	0	3	0
2	1	0	4	0
3	-1	0	1	0
4	-1	0	1	0
5	-3	0	-1	0
6	1	0	3	0
7	-1	0	2	0
8	-6	2	-8	0
Mean	-1	2	1*	4

* for p value < 0.05

Each value in the table represents the average displacement of the GHRC after 10 repetitions of arm elevation. For most specimens, regardless of whether the rotator cuff was intact or torn, the displacement of the geometric GHRC was in the same direction. On average, elevation of the arm with the rotator cuff intact caused minimal medial/lateral displacement of the GHRC (mean of -1 mm). A rotator cuff tear had a significant impact ($p=0.013$) on the GHRC displacement (average 1 mm).

6.5.3 Inferior and superior displacement of the GHRC (y-axis) after elevation of the arm, with and without an intact rotator cuff.

Table 6.3 shows the values obtained for the displacement of the geometric GHRC on the *y*-axis before and after a massive rotator cuff tear. A positive value represents a superior displacement and a negative value represents an inferior displacement relative to the initial starting position, which is set to 0. A displacement is measured in millimeters.

Table 6.3: Average inferior and superior displacement (mm) of the GHRC (*y*-axis) with and without an intact rotator cuff.

Specimen	Geometric GHRC with cuff intact (mm)	Standard Deviation (mm)	Geometric GHRC with cuff tear (mm)	Standard Deviation (mm)
1	8	0	5	0
2	8	0	10	0
3	2	0	6	0
4	7	0	12	0
5	6	0	9	0
6	3	0	6	0
7	16	0	19	0
8	13	5	18	0
Mean	8	5	10*	5

* for p value < 0.05

Each value in the table represents the average displacement of the GHRC after 10 repetitions of arm elevation. For most specimens whether the cuff was intact or torn the displacement of the geometric GHRC was in same direction. On average, elevation of the arm with the rotator cuff intact caused a superior migration of 8mm for the geometric GHRC. However, in the presence of a rotator cuff tear, we found a significantly greater superior displacement of the GHRC ($p < 0.01$). On average, the elevation of the arm with the rotator cuff tear caused a superior migration of 10 mm for the geometric GHRC.

6.5.4 Impact of a rotator cuff tear on the force required to obtain maximal elevation of the arm.

Table 6.4 shows the computed average of the means obtained of the force needed to elevate the arm for each degree of elevation.

Table 6.4 : Paired Samples Statistics.

Degree of elevation	Rotator cuff	Mean force	N	% of force needed with cuff tear	Sig. (2-tailed)
5	intact	6	8	163	.006*
	ruptured	9			
6	intact	6	8	166	.002*
	ruptured.	11			
7	intact	7	8	167	.001*
	ruptured	12			
8	intact	8	8	166	.000*
	ruptured	14			
9	intact	9	8	180	.006*
	ruptured	15			
10	intact	10	8	160	.000*
	ruptured	16			
11	intact	11	8	156	.000*
	ruptured	18			
12	intact	12	8	153	.000*
	ruptured	19			
13	intact	14	8	149	.000*
	ruptured	22			
14	intact	15	8	147	.000*
	ruptured	22			
15	intact	16	8	145	.000*
	ruptured	24			
16	intact	18	8	143	.000*
	ruptured	26			
17	intact	20	8	139	.000*
	ruptured	27			
18	intact	21	8	137	.000*
	ruptured	29			
19	intact	23	8	135	.000*
	ruptured	31			
20	intact	25	8	132	.000*
	ruptured	33			
21	intact	27	8	130	.000*
	ruptured	35			
22	intact	30	8	127	.000*
	ruptured	38			
23	intact	32	8	124	.000*
	ruptured	40			

24	intact	35	8	120	.000*
	ruptured	42			
25	intact	38	8	117	.000*
	ruptured	45			
26	intact	42	8	113	.001*
	ruptured	48			
27	intact	46	8	109	.008*
	ruptured	50			
28	intact	51	8	105	.102
	ruptured	53			
29	intact	53	7	103	.000*
	ruptured	55			
30	intact	58	7	100	.001*
	ruptured	58			
31	intact	62	7	97.7	.008*
	ruptured	61			
32	intact	64	6	96.0	.102
	ruptured	62			
33	intact	64	5	99.5	.346
	ruptured	64			
34	intact	69	5	97.4	.954
	ruptured	67			
35	intact	74	5	95.4	.569
	ruptured	71			
36	intact	73	4	91.0	.510
	ruptured	66			
37	intact	78	4	89.1	.150
	ruptured	70			
38	intact	84	4	87.5	.025*
	ruptured	73			
39	intact	89	4	86.1	.047*
	ruptured	77			
40	intact	87	3	87.5	.118
	ruptured	77			
41	intact	93	3	90.3	.269
	ruptured	84			
42	intact	98	3	92.4	.583
	ruptured	90			
43	intact	103	3	92.8	.367
	ruptured	96	3		
44	intact	107	2	91.4	.583
	ruptured	98			

* for p value < 0.05

From 5 to 28 degrees of elevation, all 8 specimens were included for comparison of the recorded force for both the intact cuff and the ruptured cuff, since all reached at least 28 degrees of elevation. From 29 degrees to 44 degrees of elevation, fewer and fewer specimens had arm elevation measurements available for

comparison for both conditions. We noticed that from 5 degrees of elevation to 30 degrees of elevation, the force required to elevate the arm is greater when the cuff is ruptured (values were over 100% of the force that was needed with intact cuff). For the first 27 degrees, the differences were significant. From 31 degrees up to 44 degrees of elevation, less force is required to elevate the arm when the cuff is ruptured (values were less than 100% of what was needed with the cuff intact). but the differences were not significant.

Figure 6.4 illustrates the differences in the force required for elevation of the arm with and without an intact cuff. The two curves intersect at around 30 degrees of elevation.

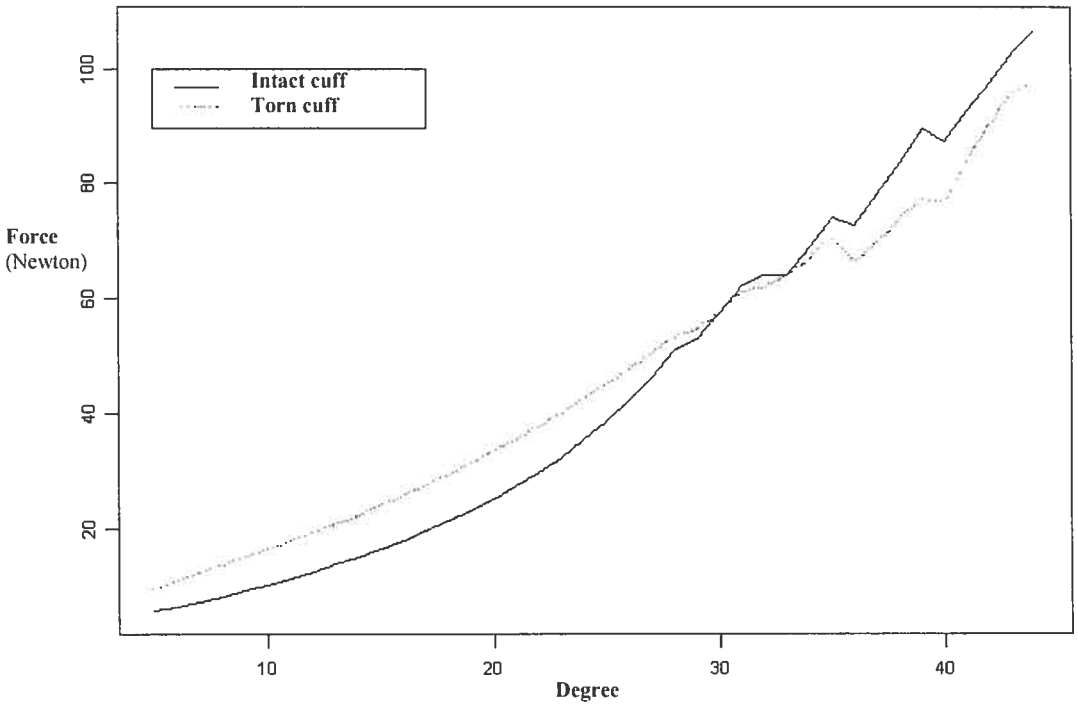

Figure 6.4: Graph showing force required for each degree of elevation.

Table 6.5 shows the mean maximal elevation obtained by each specimen with and without an intact cuff. For all specimens, except number 4, the arm elevated slightly higher when the cuff was ruptured.

Table 6.5 : Maximal elevation in degree with and without an intact rotator cuff.

Specimen	Cuff intact	Std deviation	Cuff ruptured	Std deviation
1	34.6°	0.8°	35.4°	0.6°
2	28.5°	0.2°	30.1°	0.3°
3	29.5°	0.2°	33.8°	0.3°
4	31.2°	0.3°	29.4°	10.1°
5	42.4°	0.5°	45.5°	0.4°
6	45.1°	0.2°	48.5°	0.4°
7	37.7°	0.3°	40.4°	0.3°
8	38.8°	13.7°	43.4°	0.4°
Average	36.0°	6.1°	38.3°	7.2°
p value				0.016

Interestingly, there is a significant difference between the average maximal elevations of the arm with and without an intact cuff tear. The average of the means for maximal elevation was higher for the arms with the cuff ruptured ($p < 0.05$).

6.6 Discussion

Several studies have analyzed different shoulder pathologies using *in vitro* models (Ovesen and Nielsen 1986; An, Browne et al. 1991; Loehr, Helmig et al. 1994; Debski, McMahon et al. 1995; Halder, Zhao et al. 2001; Kelkar, Wang et al. 2001; Parsons, Apreleva et al. 2002). Debski developed a sophisticated dynamic shoulder testing apparatus to examine glenohumeral joint motion in cadaveric full upper extremities(Debski, McMahon et al. 1995). This model was used to evaluate the impact of massive cuff tears on glenohumeral abduction (Thompson, Debski et al. 1996). Such tears prevented arm elevation beyond 25 degrees of glenohumeral abduction despite a threefold increase in middle deltoid force. Furthermore, in this model, a ball and socket joint kinematics is preserved until the transverse force couple is affected by paralysis or cuff tear.

In the present study, we reproduce the kinematics of a cadaver shoulder with a massive rotator cuff tear in an *in vitro* system. We used full cadaver arms with matching individualized 3D reconstructions, and recorded the 3D displacement of the glenohumeral rotation center (GHRC) during arm elevation in the scapular plane. We observed a significant lateral and superior displacement of the GHRC in the presence of a massive rotator cuff tear, but no significant displacement of the GHRC in the antero-posterior axis, compared with shoulders having an intact rotator cuff.

Maximal arm elevation in a physiological system with only gleno-humeral movement allowed is 90 degrees. Surprisingly, in our model, the mean maximal arm elevation for shoulders with an intact rotator cuff was less than 90 degrees, and slightly lower than the mean for those without an intact cuff (36.0 degrees and 38.3 degrees, respectively). This unexpected finding was statistically significant, and we believe it may be due to the non-physiologic buckling of the tissue of the intact rotator cuff at maximal shoulder elevation. This could have occurred with our model since we did not simulate the movement of the rotator cuff muscles. Therefore, the inactive cuff tissue could not move out of the joint with abduction of the arm, and at some point, physically blocked further abduction, resulting in a decreased maximal elevation. When the cuff is resected to simulate a massive tear, this blockage seems to be avoided, allowing slightly greater elevation of the arm.

Despite this intricate finding, we did find superior displacement of the GHRC and a maximal arm elevation of 35 to 40 degrees when a massive rotator cuff tear was reproduced, which corresponds to the clinical signs observed in living subjects with pseudoparalysis (Neer, Craig et al. 1983). Our model also allowed us to record the force required for each degree of arm elevation. We noted that for each degree of shoulder abduction up to 31 degrees, the force required was significantly greater when the cadaver shoulder had a massive rotator cuff tear. The difference in force required to elevate the arm past 31 degrees was not significant. In their study, Thompson and colleagues simulated a paralysis of the supraspinatus muscle, which caused a significant increase (201%) in the middle deltoid force required to initiate abduction. However, much less force was required (112%) for full abduction once the movement was initiated (Thompson, Debski et al. 1996). With a simulated massive cuff tear, they obtained a maximal abduction of 25 degrees despite a threefold increase in middle deltoid force (Thompson, Debski et al. 1996).

In our study, even though the function of the rotator cuff was not simulated during all parts of the experiment, we did find a significant increase in the force required to elevate the arm through the first 30 degrees of abduction when the cuff was resected. We conclude that the presence of the rotator cuff, even as an inert soft tissue spacer, provided a biomechanically more favorable environment for the elevation of the arm than having a massive cuff tear. This supports our hypothesis that morphological features relating to the glenohumeral joint can have an impact on joint kinematics.

We found that the greatest increase in force requirements occurred during initiation of elevation, which seems to correspond to a frequent clinical finding of CTA. Patients with a pseudoparalytic shoulder cannot initiate elevation of the arm, but once helped by the examiner to elevate the arm past the horizontal level; most patients are then able to maintain the arm elevated. Our findings suggest that we should focus our attention on modifying features about the glenohumeral joint that could decrease the force requirement for the initiation of the elevation.

Our results with regard to humeral head migration, maximal arm elevation, and deltoid force requirements for shoulder movement concur with other results published in the literature. Wuelker and colleagues used a dynamic *in vitro* shoulder model and showed that deltoid force, applied alone, results in a decrease of glenohumeral joint elevation of 25% (Wuelker, Wirth et al. 1995). Sharkey and colleagues looked at the influence of rotator cuff muscle activity on humeral head migration in five cadaver shoulders (Sharkey and Marder 1995), and found that abduction without the subscapularis, infraspinatus, and teres minor muscles causes significant superiorly directed shifts in humeral head position as does abduction using only the deltoid muscle.

Most studies of the kinematics of shoulder prostheses are retrospective clinical reviews looking for a correlation between components positioning and restoration of function. Most authors have demonstrated the importance of proper positioning of the humeral component, but few have studied *in vitro* performance of the current prostheses available on the market. Nyffeler analyzed the *in vitro* placement of the glenoid component of the reverse shoulder prosthesis, and concluded that positioning of the glenoid component with overriding of the inferior border of the osseous glenoid edge allows for significantly better adduction and abduction (Nyffeler, Werner et al. 2005). De Wilde used a 3D computer model to reproduce the biomechanical properties of 10 different prosthetic designs. He calculated the moment arm of the deltoid muscle in the scapular plane. Results show favorable kinematics for non-anatomic design. When the center of rotation is medialized, the deltoid muscle is elongated, and the deltoid lever arm is increased, such as with the reverse shoulder prosthesis(De Wilde, Audenaert et al. 2004). As suggested by De Wilde, a non-anatomic design of shoulder prosthesis may have the most potential to restore function to a shoulder with abnormal biomechanics.

In the present study, we used our *in vitro* model of shoulder movement to study the changes in shoulder kinematics caused by a massive cuff tear. We demonstrated a significant superior and lateral displacement of the GHRC in shoulders with simulated massive cuff tear. Furthermore, we have shown that the presence of the rotator cuff, even as an inactive soft tissue spacer between the acromion and humeral head, can play an important role in keeping the force requirement for initiation of arm elevation to a minimum.

Future studies to better understand the pathological kinematics of shoulders with massive rotator cuff tear may ultimately help define parameters for novel prosthetic design.

6.7 Acknowledgement

The authors would like to acknowledge the financial support of NSERC, FQRNT, and FRSQ.

Chapitre 7: Discussion générale

L'arthropathie de l'épaule secondaire à une déchirure massive de la coiffe des rotateurs (ADC) est une condition incapacitante qui sera sans doute de plus en plus prévalente avec le vieillissement de la population. Heureusement, depuis le développement de la prothèse inversée du Dr Grammont, une nouvelle option thérapeutique est disponible pour les patients(Grammont and Baulot 1993). Cet implant gagne en popularité à travers le monde, et a également capté l'attention des scientifiques. Il existe maintenant un regain d'intérêt pour la recherche fondamentale concernant la cinématique de l'épaule, et un désir d'ajouter plus de science derrière le design de nouveaux implants(De Wilde, Audenaert et al. 2004). À ce jour, la prothèse inversée est la seule qui permette de reverser la pseudoparalysie de l'ADC(Sirveaux, Favard et al. 2004; Boileau, Watkinson et al. 2005; Werner, Steinmann et al. 2005). Les contraintes liés au design de l'implant augmentent le risque de descellement et débricolage à long terme, dès lors la recommandation d'une implantation pour les 70 ans et plus.

Toutefois, il demeure intriguant que l'évolution clinique de cette condition soit si variable, et que certains patients puissent conserver un niveau inusité de fonction malgré une déchirure massive de la coiffe(Neer, Craig et al. 1983; Hamada, Fukuda et al. 1990). Différentes études biomécaniques ont expliqué l'apport en force d'une coiffe des rotateurs déchirée et la préservation de la fonction, mais peu d'études ont porté une attention particulière à l'impact des structures avoisinantes à l'articulation glénohumérale sur la préservation de la fonction. Encore de nos jours, aucun facteur pronostic n'a été identifié permettant de savoir avec certitude quelle épaule avec une déchirure de coiffe évoluera vers l'ADC. Pour permettre un jour aux chirurgiens de savoir où intervenir afin de pouvoir prévenir ou traiter la pseudoparalysie, il nous importe d'acquérir une meilleure connaissance de la cinématique de l'articulation glénohumérale en présence d'une déchirure massive de la coiffe des rotateurs.

Dans un premier temps, nous avons étudié différentes techniques d'estimation du centre de rotation glénohuméral, soit par la méthode géométrique et la méthode fonctionnelle, et les avons comparées une à l'autre. Il semble que cette étude est la première à comparer deux techniques d'estimation du centre de rotation glénohuméral. Nous avons mis en évidence que les centres de rotation étudiés ne

coïncident pas dans leurs positions et déplacements. Cette trouvaille a une certaine importance puisque le calcul du bras de levier du deltoïde n'est possible qu'en connaissance de la localisation du centre de rotation. Etant donné que ces centres de rotation ne sont pas exactement les mêmes, la valeur du bras de levier calculée peut différer.

Afin de pouvoir analyser les résultats des différentes études, il faut donc prendre en considération la technique employée pour l'estimation du centre de rotation puisqu'un changement de position du centre de rotation peut potentiellement modifier l'analyse cinématique et son interprétation. La localisation du centre de rotation est une référence pour l'analyse cinématique, et se doit d'être précise. Notre étude ne dit pas quelle technique d'estimation est préférable, mais bien que la localisation du centre de rotation peut varier selon la technique utilisée. La méthode d'estimation géométrique a été retenue pour permettre l'analyse cinématique de la dernière étude de ce mémoire.

En seconde partie, nous avons noté que l'utilisation du système de coordonnées standardisées pour l'articulation de l'épaule, défini par «l'International Society of Biomechanics (ISB)» (Wu et al. 2005), peut porter à confusion lors de l'interprétation des données. En effet, chaque spécimen avait une valeur de référence différente, quant à la position initiale du bras, malgré un positionnement similaire sur le montage. Nous avons donc décidé de comparer le système de coordonnées défini par l'ISB (Wu et al. 2005) à un système de coordonnées défini par l'alignement mathématique de ces axes.

Cette étude a permis de démontrer qu'il n'y a pas de différence dans l'amplitude de mouvement calculé peu importe le système de coordonnées utilisé. Toutefois, nous croyons que l'alignement des axes du système de coordonnées facilite l'interprétation de la cinématique 3D de l'articulation glénohumérale, puisque la position initiale de référence du bras est à 0° d'abduction, 0° de flexion horizontale et 0° de rotation pour tous les spécimens. De plus, les valeurs angulaires obtenues dans cette position semblent correspondre davantage aux valeurs notées à la position de repos du bras sur un sujet vivant. Cette méthode d'analyse avec alignement des axes du système de coordonnées a été reprise pour la dernière étude de ce mémoire.

Dans cette dernière étude, nous avons reproduit la cinématique de l'épaule avec déchirure massive de la coiffe des rotateurs. Pour chaque spécimen, nous avons observé une migration proximale de la tête humérale sous l'action non opposée du mécanisme de simulation du deltoïde, ainsi que la butée de la tête humérale contre l'acromion de l'omoplate. Nous avons observé une différence significative pour les déplacements latéral et supérieur du centre de rotation de la tête humérale chez les spécimens avec déchirure massive de la coiffe, et pas de différence significative pour le déplacement du centre de rotation dans l'axe médiolatéral. De plus, l'augmentation de la force nécessaire pour les 30° premiers degrés d'élévation du bras était statistiquement significative pour les spécimens avec déchirure de coiffe. Ceci correspond en partie à la pseudoparalysie retrouvée en clinique. Les patients sont incapables de lever le bras plus haut que 30°, mais lorsque que l'examinateur lève passivement le bras du patient, celui-ci peut maintenir le bras élevé au-dessus de la tête.

Il existe donc une phase critique dans la mécanique de l'ascension du bras, dans les premiers degrés d'élévation, sur laquelle nous croyons qu'il est possible d'intervenir afin de contrer la pseudoparalysie. Nous avons démontré, *in vitro*, que la coiffe des rotateurs, même intacte et inactive comme tissu d'interposition entre la tête humérale et l'acromion, agissait sur la cinématique glénohumérale en minimisant le besoin en force pour l'élévation du bras. Ceci nous permet de croire qu'une modification morphologique des structures avoisinantes à l'articulation glénohumérale pourrait peut-être minimiser davantage ce besoin en force.

Cette première analyse cinématique, nous a permis de conclure que notre montage expérimental reproduit bien la cinématique d'une épaule avec déchirure massive de la coiffe des rotateurs. Nous sommes très enthousiastes quant aux résultats obtenus, mais aussi conscients des limites de ces études, principalement reliées à l'utilisation de spécimens cadavériques et d'un montage expérimental. Notre montage simule l'élévation du bras dans le plan de l'omoplate seulement, mais les mouvements de l'épaule sont beaucoup complexes. Nous avons toutefois opté pour une simulation dans le plan de l'omoplate pour simplifier le montage, limiter les variables, et respecter le cadre budgétaire. Les connaissances acquises ont tout de même lancé la mise en chantier de projets complémentaires qui permettront peut-être d'identifier sur quel paramètre morphologique une intervention chirurgicale permettra le rétablissement de la fonction chez les patients atteints de l'ADC.

Références

Ahir, S. P., P. S. Walker, et al. (2004). "Analysis of glenoid fixation for a reversed anatomy fixed-fulcrum shoulder replacement." J Biomech **37**(11): 1699-708.

An, K. N., A. O. Browne, et al. (1991). "Three-dimensional kinematics of glenohumeral elevation." J Orthop Res **9**(1): 143-9.

Apoil, A. (1989). "[Degenerative lesions of the rotator cuff of the shoulder. Current status of the surgical treatment]." Chirurgie **115 Suppl 1**: 1-6.

Arntz, C. T., S. Jackins, et al. (1993). "Prosthetic replacement of the shoulder for the treatment of defects in the rotator cuff and the surface of the glenohumeral joint." J Bone Joint Surg Am **75**(4): 485-91.

Arntz, C. T., F. A. Matsen, 3rd, et al. (1991). "Surgical management of complex irreparable rotator cuff deficiency." J Arthroplasty **6**(4): 363-70.

Bankes, M. J. and R. J. Emery (1995). "Pioneers of shoulder replacement: Themistocles Gluck and Jules Emile Pean." J Shoulder Elbow Surg **4**(4): 259-62.

Baumgarten, K. M., C. J. Lashgari, et al. (2004). "Glenoid resurfacing in shoulder arthroplasty: indications and contraindications." Instr Course Lect **53**: 3-11.

Bigliani, L. U., R. Kelkar, et al. (1996). "Glenohumeral stability. Biomechanical properties of passive and active stabilizers." Clin Orthop Relat Res(330): 13-30.

Boileau, P. and G. Walch (1997). "The three-dimensional geometry of the proximal humerus. Implications for surgical technique and prosthetic design." J Bone Joint Surg Br **79**(5): 857-65.

Boileau, P., D. J. Watkinson, et al. (2005). "Grammont reverse prosthesis: design, rationale, and biomechanics." J Shoulder Elbow Surg **14**(1 Suppl S): 147S-161S.

Burkhart, S. S. (1992). "Fluoroscopic comparison of kinematic patterns in massive rotator cuff tears. A suspension bridge model." Clin Orthop Relat Res(284): 144-52.

Burkhart, S. S., J. C. Esch, et al. (1993). "The rotator crescent and rotator cable: an anatomic description of the shoulder's "suspension bridge"." Arthroscopy **9**(6): 611-6.

Burkhart, S. S., W. M. Nottage, et al. (1994). "Partial repair of irreparable rotator cuff tears." Arthroscopy **10**(4): 363-70.

Caporali, R., S. Rossi, et al. (1994). "Tidal irrigation in Milwaukee shoulder syndrome." J Rheumatol **21**(9): 1781-2.

Cofield, R. H. and B. T. Briggs (1979). "Glenohumeral arthrodesis. Operative and long-term functional results." J Bone Joint Surg Am **61**(5): 668-77.

Coughlin, M. J., J. M. Morris, et al. (1979). "The semiconstrained total shoulder arthroplasty." J Bone Joint Surg Am **61**(4): 574-81.

Culham, E. and M. Peat (1993). "Functional anatomy of the shoulder complex." J Orthop Sports Phys Ther **18**(1): 342-50.

de Leest, O., P. M. Rozing, et al. (1996). "Influence of glenohumeral prosthesis geometry and placement on shoulder muscle forces." Clin Orthop Relat Res(330): 222-33.

De Wilde, L. F., E. A. Audenaert, et al. (2004). "Shoulder prostheses treating cuff tear arthropathy: a comparative biomechanical study." J Orthop Res **22**(6): 1222-30.

Debski, R. E., P. J. McMahon, et al. (1995). "A new dynamic testing apparatus to study glenohumeral joint motion." J Biomech **28**(7): 869-74.

Della Vallee, C. J., A. S. Rokito, et al. (2001). Biomechanics of the Shoulder. Basic Biomechanics of the Musculoskeletal System. M. Nordin and V. H. Frankle. Baltimore, Lippincott Williams & Wilkins: 328-339.

Feeney, M. S., J. O'Dowd, et al. (2003). "Glenohumeral articular cartilage changes in rotator cuff disease." J Shoulder Elbow Surg **12**(1): 20-3.

Fenlin, J. M., Jr., J. M. Chase, et al. (2002). "Tuberoplasty: creation of an acromiohumeral articulation-a treatment option for massive, irreparable rotator cuff tears." J Shoulder Elbow Surg **11**(2): 136-42.

Field, L. D., D. M. Dines, et al. (1997). "Hemiarthroplasty of the shoulder for rotator cuff arthropathy." J Shoulder Elbow Surg **6**(1): 18-23.

Frankle, M., S. Siegal, et al. (2005). "The Reverse Shoulder Prosthesis for glenohumeral arthritis associated with severe rotator cuff deficiency. A minimum two-year follow-up study of sixty patients." J Bone Joint Surg Am **87**(8): 1697-705.

Franklin, J. L., W. P. Barrett, et al. (1988). "Glenoid loosening in total shoulder arthroplasty. Association with rotator cuff deficiency." J Arthroplasty **3**(1): 39-46.

Goutallier, D., J. M. Postel, et al. (1994). "Fatty muscle degeneration in cuff ruptures. Pre- and postoperative evaluation by CT scan." Clin Orthop Relat Res(304): 78-83.

Goutallier, D., J. M. Postel, et al. (2003). "Influence of cuff muscle fatty degeneration on anatomic and functional outcomes after simple suture of full-thickness tears." J Shoulder Elbow Surg **12**(6): 550-4.

Grammont, P. M. and E. Baulot (1993). "Delta shoulder prosthesis for rotator cuff rupture." Orthopedics **16**(1): 65-8.

Grood, E. S. and W. J. Suntay (1983). "A joint coordinate system for the clinical description of three-dimensional motions: application to the knee." J Biomech Eng **105**(2): 136-44.

Halder, A. M., K. D. Zhao, et al. (2001). "Dynamic contributions to superior shoulder stability." J Orthop Res **19**(2): 206-12.

Hamada, K., H. Fukuda, et al. (1990). "Roentgenographic findings in massive rotator cuff tears. A long-term observation." Clin Orthop(254): 92-6.

Harman, M., M. Frankle, et al. (2005). "Initial glenoid component fixation in "reverse" total shoulder arthroplasty: a biomechanical evaluation." J Shoulder Elbow Surg **14**(1 Suppl S): 162S-167S.

Helm, F. C. T. V. D., H. E. J. Veeger, et al. (1992). "Geometry parameters for musculoskeletal modelling of the shoulder system." J Biomech **25**: 129-144.

Howell, S. M. and B. J. Galinat (1989). "The glenoid-labral socket. A constrained articular surface." Clin Orthop Relat Res(243): 122-5.

Howell, S. M. and T. A. Kraft (1991). "The role of the supraspinatus and infraspinatus muscles in glenohumeral kinematics of anterior should instability." Clin Orthop Relat Res(263): 128-34.

Hsu, H. C., Z. P. Luo, et al. (2003). "Correlation between rotator cuff tear and glenohumeral degeneration." Acta Orthop Scand **74**(1): 89-94.

Inman, V. T., J. B. Saunders, et al. (1996). "Observations of the function of the shoulder joint. 1944." Clin Orthop Relat Res(330): 3-12.

Karduna, A. R., G. R. Williams, et al. (1996). "Kinematics of the glenohumeral joint: influences of muscle forces, ligamentous constraints, and articular geometry." J Orthop Res **14**(6): 986-93.

Kelkar, R., V. M. Wang, et al. (2001). "Glenohumeral mechanics: a study of articular geometry, contact, and kinematics." J Shoulder Elbow Surg **10**(1): 73-84.

Lettin, A. W., S. A. Copeland, et al. (1982). "The Stanmore total shoulder replacement." J Bone Joint Surg Br **64**(1): 47-51.

Levasseur, A., P. Tétreault, et al. (2006). "Simplification of the ISB joint coordinate system to describe shoulder kinematics." clin Biomech (Bristol, Avon), submitted.

Loehr, J. F., P. Helmig, et al. (1994). "Shoulder instability caused by rotator cuff lesions. An in vitro study." Clin Orthop(304): 84-90.

Low, J. and A. Reed (1996). Some biomechanical explanation. Basic Biomechanis Explained. J. Low and A. Reed. Oxford, Education and Professional Publishing**:** 218-250.

Marin, F., H. Mannel, et al. (2003). "Correction of axis misalignment in the analysis of knee rotations." Hum Mov Sci **22**(3): 285-96.

Matsen, F. A. (2002). "Rotator Cuff Relevant Anatomy and Mechanics." University of Washington, Orthopoedics & Sports Medicine.

McFarland, E. G., P. Sanguanjit, et al. (2006). "The reverse shoulder prosthesis: a review of imaging features and complications." Skeletal Radiol **35**(7): 488-96.

McMahon, P. J., R. E. Debski, et al. (1995). "Shoulder muscle forces and tendon excursions during glenohumeral abduction in the scapular plane." J Shoulder Elbow Surg **4**(3): 199-208.

Meskers, C. G., F. C. van der Helm, et al. (1998). "In vivo estimation of the glenohumeral joint rotation center from scapular bony landmarks by linear regression." J Biomech **31**(1): 93-6.

Murphy, L. A. and P. J. Prendergast (2005). "Acromion-fixation of glenoid components in total shoulder arthroplasty." J Biomech **38**(8): 1702-11.

Neer, C. S., 2nd (1963). "Prosthetic Replacement of the Humeral Head: Indications and Operative Technique." Surg Clin North Am **43**: 1581-97.

Neer, C. S., 2nd (1974). "Replacement arthroplasty for glenohumeral osteoarthritis." J Bone Joint Surg Am **56**(1): 1-13.

Neer, C. S., 2nd, E. V. Craig, et al. (1983). "Cuff-tear arthropathy." J Bone Joint Surg Am **65**(9): 1232-44.

Neer, C. S., 2nd, K. C. Watson, et al. (1982). "Recent experience in total shoulder replacement." J Bone Joint Surg Am **64**(3): 319-37.

Nove-Josserand, L., C. Levigne, et al. (1996). "[The acromio-humeral interval. A study of the factors influencing its height]." Rev Chir Orthop Reparatrice Appar Mot **82**(5): 379-85.

Nyffeler, R. W., C. M. Werner, et al. (2005). "Biomechanical relevance of glenoid component positioning in the reverse Delta III total shoulder prosthesis." J Shoulder Elbow Surg **14**(5): 524-8.

Nyffeler, R. W., C. M. Werner, et al. (2004). "Analysis of a retrieved delta III total shoulder prosthesis." J Bone Joint Surg Br **86**(8): 1187-91.

Orr, T. E., D. R. Carter, et al. (1988). "Stress analyses of glenoid component designs." Clin Orthop Relat Res(232): 217-24.

Ovesen, J. and S. Nielsen (1986). "Anterior and posterior shoulder instability. A cadaver study." Acta Orthop Scand **57**(4): 324-7.

Parsons, I. M., M. Apreleva, et al. (2002). "The effect of rotator cuff tears on reaction forces at the glenohumeral joint." J Orthop Res **20**(3): 439-46.

Poppen, N. K. and P. S. Walker (1976). "Normal and abnormal motion of the shoulder." J Bone Joint Surg Am **58**(2): 195-201.

Post, M. (1985). "Constrained total shoulder replacement." Instr Course Lect **34**: 287-94.

Post, M., S. S. Haskell, et al. (1980). "Total shoulder replacement with a constrained prosthesis." J Bone Joint Surg Am **62**(3): 327-35.

Rockwood, C. A., Jr., G. R. Williams, Jr., et al. (1995). "Debridement of degenerative, irreparable lesions of the rotator cuff." J Bone Joint Surg Am **77**(6): 857-66.

Saha, A. K. (1971). "Dynamic stability of the glenohumeral joint." Acta Orthop Scand **42**(6): 491-505.

Scheibel, M., S. Lichtenberg, et al. (2004). "Reversed arthroscopic subacromial decompression for massive rotator cuff tears." J Shoulder Elbow Surg **13**(3): 272-8.

Schibany, N., H. Zehetgruber, et al. (2004). "Rotator cuff tears in asymptomatic individuals: a clinical and ultrasonographic screening study." Eur J Radiol **51**(3): 263-8.

Senk, M. and L. Cheze (2006). "Rotation sequence as an important factor in shoulder kinematics." Clin Biomech (Bristol, Avon) **21 Suppl 1**: S3-8.

Sharkey, N. A. and R. A. Marder (1995). "The rotator cuff opposes superior translation of the humeral head." Am J Sports Med **23**(3): 270-5.

Sirveaux, F., L. Favard, et al. (2004). "Grammont inverted total shoulder arthroplasty in the treatment of glenohumeral osteoarthritis with massive rupture of the cuff. Results of a multicentre study of 80 shoulders." J Bone Joint Surg Br **86**(3): 388-95.

Siston, R. A. and S. L. Delp (2006). "Evaluation of a new algorithm to determine the hip joint center." J Biomech **39**(1): 125-30.

Skalli, W., F. Lavaste, et al. (1995). "Quantification of three-dimensional vertebral rotations in scoliosis: what are the true values?" Spine **20**(5): 546-53.

Terry, G. C. and T. M. Chopp (2000). "Functional Anatomy of the Shoulder." J Athl Train **35**(3): 248-255.

Thompson, W. O., R. E. Debski, et al. (1996). "A biomechanical analysis of rotator cuff deficiency in a cadaveric model." Am J Sports Med **24**(3): 286-92.

Veeger, H. E. (2000). "The position of the rotation center of the glenohumeral joint." J Biomech **33**(12): 1711-5.

Visotsky, J. L., C. Basamania, et al. (2004). "Cuff tear arthropathy: pathogenesis, classification, and algorithm for treatment." J Bone Joint Surg Am **86-A Suppl 2**: 35-40.

Werner, C. M., P. A. Steinmann, et al. (2005). "Treatment of painful pseudoparesis due to irreparable rotator cuff dysfunction with the Delta III reverse-ball-and-socket total shoulder prosthesis." J Bone Joint Surg Am **87**(7): 1476-86.

Williams, G. R., Jr. and C. A. Rockwood, Jr. (1996). "Hemiarthroplasty in rotator cuff-deficient shoulders." J Shoulder Elbow Surg **5**(5): 362-7.

Woltring, H. J. (1990). Data processing and error analysis. Biomechanics of Human Mouvement, Application in Rehabilitation, Sport and Ergonomics. A. Capozzo and P. Berm. Washington: 203-237.

Woodruff, M. J., A. P. Cohen, et al. (2003). "Arthroplasty of the shoulder in rheumatoid arthritis with rotator cuff dysfunction." Int Orthop **27**(1): 7-10.

Wu, G., F. C. van der Helm, et al. (2005). "ISB recommendation on definitions of joint coordinate systems of various joints for the reporting of human joint motion--Part II: shoulder, elbow, wrist and hand." J Biomech **38**(5): 981-992.

Wuelker, N., H. Schmotzer, et al. (1994). "Translation of the glenohumeral joint with simulated active elevation." Clin Orthop Relat Res(309): 193-200.

Wuelker, N., C. J. Wirth, et al. (1995). "A dynamic shoulder model: reliability testing and muscle force study." J Biomech **28**(5): 489-99.

Yamaguchi, K., J. S. Sher, et al. (2000). "Glenohumeral motion in patients with rotator cuff tears: a comparison of asymptomatic and symptomatic shoulders." J Shoulder Elbow Surg **9**(1): 6-11.

Zeman, C. A., M. A. Arcand, et al. (1998). "The rotator cuff-deficient arthritic shoulder: diagnosis and surgical management." J Am Acad Orthop Surg **6**(6): 337-48.

Zuckerman, J. D., A. J. Scott, et al. (2000). "Hemiarthroplasty for cuff tear arthropathy." J Shoulder Elbow Surg **9**(3): 169-72.